University of Mississippi
eGrove

Honors Theses

Honors College (Sally McDonnell Barksdale Honors College)

2015

Design and Synthesis of Sigma-1 Probe for Positron Emission Tomography (PET) Imaging

May Ly
University of Mississippi. Sally McDonnell Barksdale Honors College

Follow this and additional works at: https://egrove.olemiss.edu/hon_thesis

 Part of the Biochemical and Biomolecular Engineering Commons

Recommended Citation
Ly, May, "Design and Synthesis of Sigma-1 Probe for Positron Emission Tomography (PET) Imaging" (2015). *Honors Theses*. 679.
https://egrove.olemiss.edu/hon_thesis/679

This Undergraduate Thesis is brought to you for free and open access by the Honors College (Sally McDonnell Barksdale Honors College) at eGrove. It has been accepted for inclusion in Honors Theses by an authorized administrator of eGrove. For more information, please contact egrove@olemiss.edu.

DESIGN AND SYNTHESIS OF SIGMA-1 PROBE FOR POSITRON EMISSION TOMOGRAPHY (PET) IMAGING

by
May May Ly

A thesis submitted to the faculty of The University of Mississippi in partial fulfillment of the requirements of the Sally McDonnell Barksdale Honors College.

Oxford
May 2015

Approved by

_____
Advisor: Dr. Christopher McCurdy

_____
Reader: Dr. Stephen Cutler

_____
Reader: Dr. Donna West-Strum

© 2015
May May Ly
ALL RIGHTS RESERVED

ACKNOWLEDGEMENTS

I would like to acknowledge Dr. Christopher McCurdy. I could never express enough appreciation for his support of this project. I approached him nearly two years ago, and he welcomed me into his research laboratory with open arms. He welcomed me into my research the entire way and has provided encouragement and motivation when I needed it most. Without his overall supervision, this project would not have been possible.

I would like to thank my second and third readers, Dr. Stephen Cutler and Dr. Donna West-Strum respectively. I appreciate their time and valuable input toward this project.

I would also like to acknowledge Mr. Walid Alsharif for his guidance and patience in training me for the type of work involved in this project. Additionally, I would also like to acknowledge the remainder of Dr. McCurdy's research laboratory group for addressing questions concerning this project.

I would like to acknowledge The University of Mississippi School of Pharmacy and Sally McDonnel Barksdale Honors College. The academic challenges and developmental opportunities throughout the past four years have made this project possible. The constant search for knowledge challenged and inspired me to work hard throughout my undergraduate career.

I am greatly appreciative for the endless support and encouragement from my friends and family.

ABSTRACT
MAY MAY LY: Design and Synthesis of Sigma-1 Probe for Positron Emission Tomography (PET) Imaging
(Under the direction of Dr. Christopher McCurdy)

Sigma-1 receptor radioligands have the potential to detect and monitor various neurological diseases. Because sigma-1 receptors are believed to be associated with numerous psychiatric conditions and neurodegenerative diseases, radioligands for sigma-1 receptors have the potential to serve as novel diagnostic tools and may be useful in assessing treatment effectiveness. A benzothiazolone ^{18}F-labeled sigma-1 receptor ligand, CM304, has demonstrated promise as a specific positron emission tomography radiotracer for visualizing sigma-1 receptors in living subjects. Based on CM304, backup molecules were created to improve the overall drug profile, including half- life and bioavailability.

TABLE OF CONTENTS

ABSTRACT ..... **IV**

LIST OF FIGURES ..... **VI**

INTRODUCTION **1**

BACKGROUND **5**

CHEMISTRY **15**

CONCLUSIONS **27**

EXPERIMENTAL **28**

REFERENCES **37**

APPENDICES **41**

LIST OF FIGURES

Figure 1	SN56
Figure 2	CM304
Figure 3	Cell uptake results for [^{18}F]CM304 and [^{3}H](+)-pentazocine
Figure 4	Time-activity curves from mouse positron emission tomography studies
Figure 5	Sagittal mouse PET images and ex vivo autoradiography of sagittal brain sections obtained 60 minutes after administration of [^{18}F]CM304
Figure 6	Rat brain PET/CT and ex vivo autoradiography
Figure 7	Monkey brain PET/MR images from baseline dynamic imaging
Figure 8	Scheme 1
Figure 9	Friedel-Crafts Acylation
Figure 10	Scheme 2
Figure 11	Scheme 3
Figure 12	Electron Pushing Mechanism
Figure 13	Available PET Tracers for Sigma 1

INTRODUCTION

A potential biomarker associated with nerve injury and neuroinflammation is the sigma-1 receptor. Sigma receptors were originally thought to belong to the opioid class of receptors (Martin, 1976). Based on the psychotomimetic effects of (±)-SKF-10,047(N-allylnormetazocine) and related benzomorpahns, which were not reversed by opioid antagonists, Martin and co-workers named this distinct class of receptor as 'sigma', derived from the first letter 'S' from SKF-10,047. It was then believed that sigma receptor sites were identical to N-methyl-D-aspartate (NMDA) receptor/phencyclidine (PCP) sites. This hypothesis was contradicted by studies using selective NMDA ligands (Wong, 1988). Therefore, sigma receptors were then classified as a unique protein family. Two known sigma receptor subtypes exist: sigma-1 and sigma-2. Of the two subtypes, sigma-1 receptors are the most well-characterized because of the receptor sequence information and availability of selective sigma-1 ligands. The sigma-1 receptor is a 25-29 kDa chaperone protein that is made up of 223 amino acids; it has been purified and cloned from several species, including mouse, rat, guinea pig, and human (Hanner, 1996; Mei, 2001; Pan, 1998; Seth, 1997; Seth, 1998). The protein shows no resemblance to other known mammalian proteins; however, it has a 30% identity and 66% homology to ergosterol-Δ^8/Δ^7-isomerase enzyme. Sigma-1 receptors do not possess sterol isomerase activity though. It is believed that the receptor has two transmembrane-spanning regions in the regions of amino acids 13 to 34 and 86 to 108, with the NH_2 and COOH ends both facing the interior of the cell.

Sigma-1 receptors are expressed throughout the body, including the heart, spleen, brain, liver, gastrointestinal tract, kidney, adrenal glands, and reproductive organs. Research has demonstrated that sigma-1 receptors are heavily concentrated within the brain; they are predominately expressed in the specific areas associated with memory, emotion, sensory functions, and motor functions (Cobos, 2008). The chief function of sigma-1 receptors is the modulatory role on dopamine, acetylcholine, N-methyl-D-aspartate, and opioid receptors (Bowen, 2000).

Mainly located at the endoplasmic reticulum of cells, sigma-1 receptors have been associated with a host of biochemical processes and pathological conditions including neurodegenerative diseases, psychiatric disorders, pain sensitization, drug addiction, digestive function, regulation of smooth muscle contraction, and ischemia (James, 2012). In most known cancers (e.g., breast, lung, colon, ovarian, prostate, brain), sigma-1 receptors are highly expressed. Sigma-1 receptors can regulate various ion channels, including potassium channels, calcium channels, dopamine and gamma-amino butyric acid (GABA) receptors thereby impacting neural excitability and transmission by affecting the release of several neurotransmitters. These neurotransmitters include: serotonin, dopamine, noradrenaline, glutamate, and GABA. Sigma-1 receptors appear to play a significant role in pain modulation and are involved in “memorizing” pain by synaptic plasticity and central sensitization. This mechanism is responsible for the chronic and self-perpetuating nature of certain pain conditions.

Certain sigma-1 receptors agonists have also been shown to control endothelial cell proliferation, improve cognition, provide neuroprotection, and act as antidepressant agents, while antagonists inhibit cocaine-induced seizures and lessen neuropathic pain,

highlighting the potential of sigma-1 receptors as both a diagnostic and therapeutic target (James, 2012). Over the past couple decades, several groups have reported the development of high affinity sigma-1 receptor ligands, and of these, some have been labeled with radioisotopes for use in positron emission tomography (PET) studies to determine the origin of pain.

Current clinical imaging methods used to evaluate chronic pain, including computed tomography (CT), ultrasound imaging (US), and magnetic resonance imaging (MRI), are primarily focused on imaging anatomic alteration, which do not necessarily reflect the origin of chronic pain (Jarvik, 2004). Various limitations in determining cause and location of nerve injury are associated with these tests. These limitations include, but are not restricted to: invasiveness, propensity to technical and operator-dependent errors, and/or lack of sufficient sensitivity and specificity to diagnose nerve injury (Shen, 2015). PET is an analytical imaging technology developed to use compounds labeled with positron emitting radioisotopes as molecular probes to image and measure biochemical processes of mammalian biology in vivo, which allows the development of instruments with high-resolution along with high sensitivity (Phelps, 2000). Radioisotopes of oxygen (^{14}O, ^{15}O), nitrogen (^{13}N), carbon (^{11}C), and most commonly fluorine (^{18}F) can be administered to a subject and detected externally are all positron emitters.

Molecular probes for PET are first developed by identifying a target process to be studied and then making a positron labeled molecule through which an assay can be performed. Because PET cannot provide direct chemical analysis of reaction products in tissue, labeled molecules are used that trace a small number of steps of biochemical process so that kinetic analysis can be used to estimate the concentration of reactants and

products over time and, from this, reaction rates (Phelps, 2000). Biochemists develop molecular probes to isolate and accurately measure a limited number of steps in a biochemical pathway. Drugs are designed to have limited interactions because the goal is to modify the function of a key step in a biological process with minimal interaction with other processes.

Before any PET procedure can become an important clinical tool, PET is a nuclear medicine technique which requires the combination of a number of factors. These factors include: (1) the necessary radioisotope has to be available on a daily basis, (2) an imaging device must give good performance for the isotope of choice, and (3) the combination of a radiopharmaceutical and a patient population for which the PET scan provides significant diagnostic information in which is not readily available with other techniques (Muehllehner, 2006). PET whole body imaging has the potential to identify early disease, differentiate benign from malignant lesions, examine all organs for metastases, and determine therapeutic effectiveness (Phelps, 2000). PET, biological, and pharmaceutical sciences are merging together with common goals of building molecules that can be used to image and measure biological functions within organ systems in living subjects, and as drugs to modify the malfunction of disease. PET could potentially provide more direct pathways from biology to the patient and link PET and pharmaceutical sciences in molecular diagnostics and molecular therapeutics, especially in various neurological diseases.

BACKGROUND

Examining sigma-1 receptors in living subjects with positron emission tomography (PET) is an important step toward understanding the receptor's functional role and involvement in disease. PET radioligands specific for sigma-1 receptors could possibly provide a noninvasive means of (1) investigating the distribution and function in both normal and disease states in living subjects, (2) assessing receptor occupancy to determine optimal doses of therapeutic drugs, (3) early detection and staging of sigma-1 receptor-related diseases, and (4) monitoring therapeutic response (James, 2012). In 2005, Yous and colleagues reported what has now been identified as a lead compound from the benzothiazolone class of compounds, SN56 (shown in Figure 1), with the aim of synthesizing a new, selective fluorinated PET radioligand for studying sigma-1 receptors in living subjects. SN56 has demonstrated high affinity and apparent high selectivity for the sigma-1 receptor.

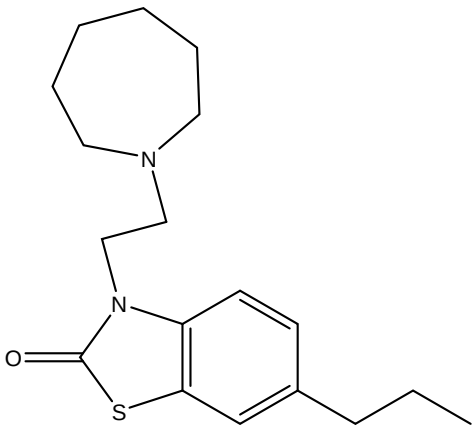

Figure 1: **SN56**

James and colleagues modified SN56 so that it could incorporate fluorine-18 radiolabel without greatly altering the structure of the molecule in hopes of maintaining its high affinity and selectivity for the sigma-1 receptor. The target molecule, 6-(3-fluropropyl)-3-(2-(azepan-1-yl)ethyl)benzo[d]thiazol-2(3H)-one, contains a fluoropropyl in place of the propyl group of SN56. This compound can also be referenced as CM304 (shown in Figure 2).

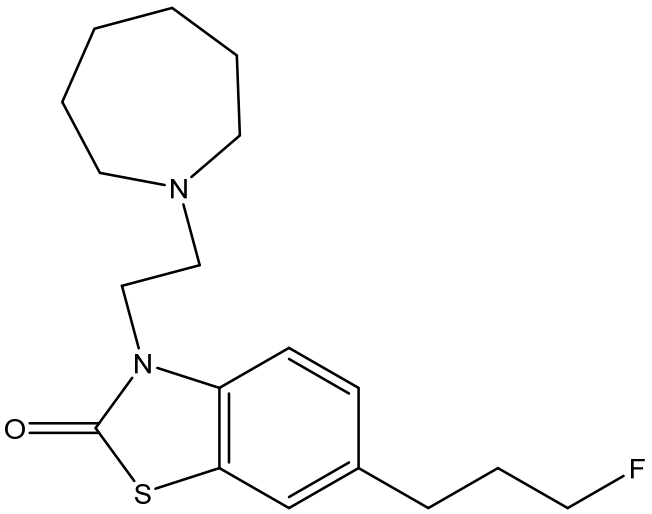

Figure 2: **CM304**

Through radioligand binding assays, CM304 demonstrated high affinity and superior selectivity for sigma-1 receptors in rat brain homogenates. Initially, binding assays were performed using brain homogenates because the central nervous system is a primary destination for the radiotracer being developed; however, the compounds were also tested in the liver. In a NovaScreen and in-house profile of 59 targets, CM304 displayed greater than 10,000-fold selectivity for sigma-1 receptor compared to all other tested targets (James, 2012).

CM304 was radiolabelled with fluorine-18 in order to trace the compound in living subjects. The uptake of this radioactive compound in Chinese hamster ovary cells was compared to the uptake of the known sigma-1 receptor ligand [^{3}H](+)-pentazocine. Control Chinese hamster ovary cells cells were transfected with a vector not containing the sigma-1 receptor gene, while the experimental Chinese hamster ovary cells were transfected with a vector containing sigma-1 receptor cDNA, which serves as a positive control for sigma-1 receptor expression in cells. Cells were exposed to [^{18}F]CM304 or [^{3}H](+)-pentazocine for 30 and 120 minutes. According to the data, there was a slight increase in uptake for both radioligands between 30 minutes and 120 minutes in control Chinese hamster ovary cells (James, 2012). In the Chinese hamster ovary cells transfected with sigma-1 receptor cDNA, this increase was more profound and numerically higher at both 30 minutes and 120 minutes than the control Chinese hamster ovary cells. At 120 minutes, the uptake of [^{18}F]CM304 in the experimental cells was 4-fold higher than uptake in control Chinese hamster ovary cells as seen in Figure 3.

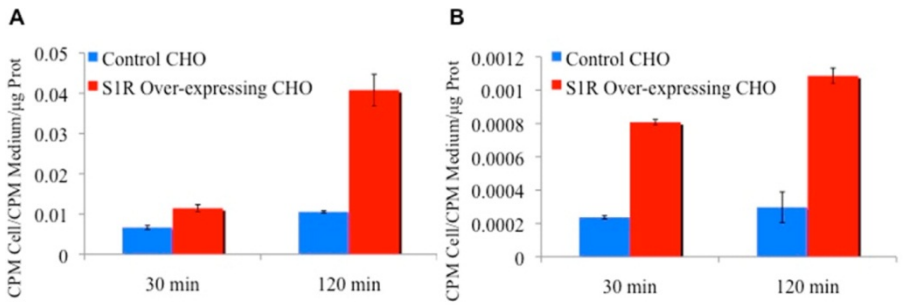

Figure 3: **Cell uptake results for [^{18}F]CM304 and [^{3}H](+)-pentazocine**. Results are expressed as counts per minute recorded in a sample from a particular cell per counts per minute recorded in medium per amount of protein (µg) present in a sample from that well.
Reprinted with permission from James, M. L.; Shen, B.; Zavaleta, C. L.; Nielsen, C. H.; Mesangeau, C.; Vuppala, P. K.; Chan, C.; Avery, B. A.; Fishback, J. A.; Matsumoto, R. R.; Gambhir, S. S.; McCurdy, C. R.; Chin, F. T. New positron emission tomography (PET) radioligand for imaging sigma-1 receptors in living subjects. *J Med Chem.* 2012, 55, 8272-8282. Copyright 2015 American Chemical Society.

Small animal PET was used to assess the in vivo kinetics of [^{18}F]CM304 in normal mice. Brain PET scanning began 1 minute before the administration of [^{18}F]CM304 and stopped 60 minutes later. The baseline time-activity curve, shown in Figure 4, demonstrates that [^{18}F]CM304 entered the brain quickly, spiked within the first few minutes, and then gradually decreased over the remaining time of the scan. [^{18}F]CM304 reached its maximum uptake in mouse brain within the first few minutes of imaging and gradually washed out to 65% of its maximum at 60 minutes after the administration.

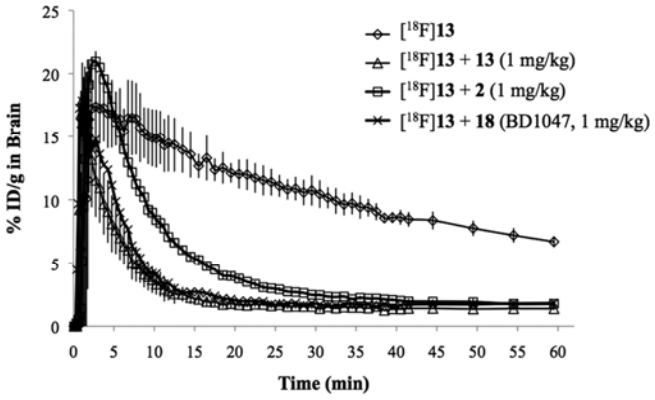

Figure 4: **Time-activity curves (TACs) from mouse positron emission tomography studies.** TACs represent accumulation of [^{18}F]CM304 in whole mouse brain as a function of time for baseline, preblock with haloperidol, preblock with FTC-146, and preblock with [^{18}F]FTC-146.
Reprinted with permission from James, M. L.; Shen, B.; Zavaleta, C. L.; Nielsen, C. H.; Mesangeau, C.; Vuppala, P. K.; Chan, C.; Avery, B. A.; Fishback, J. A.; Matsumoto, R. R.; Gambhir, S. S.; McCurdy, C. R.; Chin, F. T. New positron emission tomography (PET) radioligand for imaging sigma-1 receptors in living subjects. *J Med Chem.* 2012, 55, 8272-8282. Copyright 2015 American Chemical Society.

PET images provided visual evidence that [^{18}F]CM304 rapidly crossed the blood-brain barrier and appeared to accumulate in known sigma-1 receptor rich regions. An accurate depiction of radioligand localization in specific brain regions could not be determined solely with PET; therefore, ex vivo autoradiography was performed. Results from the autoradiography demonstrated that [^{18}F]CM304 accumulated in the midbrain,

facial nucleus, cortex, and hippocampus and to a lesser extent in the cerebellum and thalamus (shown in Figure 5).

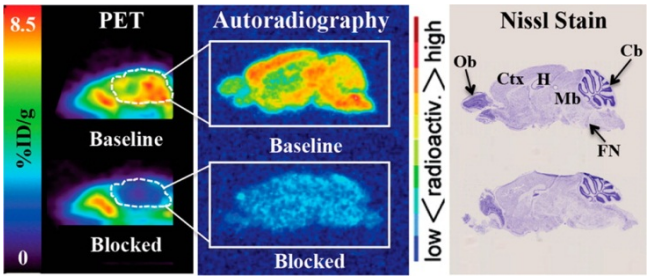

Figure 5: **PET images and ex vivo autoradiography of sagittal brain sections (12 µm) obtained 60 minutes after administration of [^{18}F]CM304**. Sections used for autoradiography were stained with Nissl for anatomical correlation. PET images were acquired just before to perfusing mice and harvesting brain tissue for autoradiography. White dotted lines designate location of mouse brain in sagittal PET images: Cb = cerebellum, Ctx = cortex, FN = facial nucleus, H = hippocampus, Mb = midbrain, Ob = olfactory bulb.

Reprinted with permission from James, M. L.; Shen, B.; Zavaleta, C. L.; Nielsen, C. H.; Mesangeau, C.; Vuppala, P. K.; Chan, C.; Avery, B. A.; Fishback, J. A.; Matsumoto, R. R.; Gambhir, S. S.; McCurdy, C. R.; Chin, F. T. New positron emission tomography (PET) radioligand for imaging sigma-1 receptors in living subjects. *J Med Chem.* 2012, 55, 8272-8282. Copyright 2015 American Chemical Society.

[^{18}F]CM304 was further assessed in rats and squirrel monkeys by James and colleagues. Rats were administered [^{18}F]CM304 intravenously, and static PET scans were measured after 50 minutes. For blocking studies, rats were pretreated with BD1047 ten minutes before tracer administration. A CT image was acquired after each PET scan to provide an anatomic reference frame for the respective PET data. The rats were sacrificed after PET imaging, and the brains were removed, which allowed for autoradiography to be performed.

Baseline PET/CT images (shown in Figure 6) again demonstrated [^{18}F]CM304's ability to cross the blood-brain barrier and accumulate in brain tissue. The PET/CT images also revealed some accumulation of radioactivity in the rat skull. Accumulation of [^{18}F]CM304 was found in the brain stem, cerebellum, cortex, hypothalamus, nucleus oculomotor, red nucleus, thalamus, caudate putamen, and hippocampus. There was little

uptake of [^{18}F]CM304 in the corpus callosum and muscle. Both blocking studies showed a reduction in the uptake of [^{18}F]CM304.

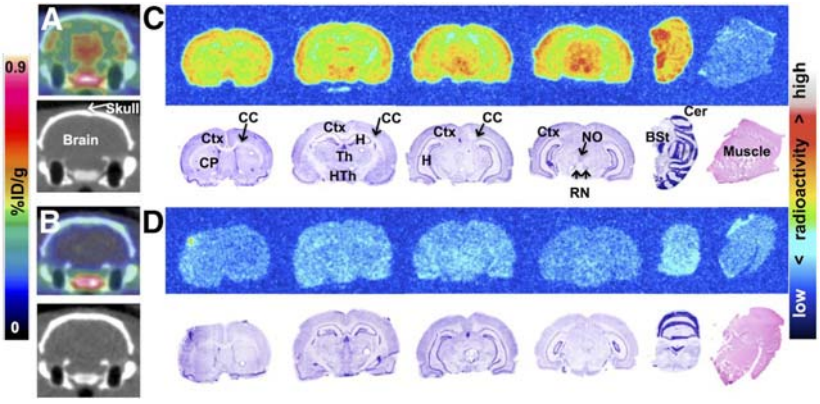

Figure 6: **Rat brain PET/CT and ex vivo autoradiography**. (A) Baseline coronal PET/CT images 50-60 minutes after intravenous administration of [^{18}F]CM304. (B) PET/CT images from blocking study. (C) Autoradiography and nissl/H&E staining of coronal brain and muscle sections from baseline study. (D) Autoradiography and nissl/H&E staining of coronal brain and muscle sections from blocking studies. Bst = brain stem; CC = corpus callosum; Cer = cerebellum; CP = caudate-putamen; Ctx = cortex; H = hippocampus; HTh = hypothalamus; NO = nucleus oculomotor; RN = red nucleus; Th = thalamus.
This research was originally published in *JNM*. Evaluation of σ-1 James, M. L.; Shen, B.; Nielsen, C. H.; Behera, D.; Buckmaster, C. L.; Mesangeau, C.; Zavaleta, C.; Vuppala, P. K.; Jamalapuram, S.; Avery, B. A.; Lyons, D. M.; McCurdy, C. R.; Biswal, S.; Gambhir, S. S.; Chin, F. T. Evaluation of σ-1 receptor radioligand ^{18}F-FTC-146 in rats and squirrel monkeys using PET. *J Nucl Med*. 2014, 55, 147-153. © by the Society of Nuclear Medicine and Molecular Imaging, Inc.

Preliminary brain PET imaging of squirrel monkeys was performed to evaluate the regional distribution and brain permeability of [^{18}F]CM304 in a nonhuman primate. A total of four brain PET images were obtained. The monkeys were injected intravenously with [^{18}F]CM304 in 500 microliters of sterile heparinized saline, followed by 500 microliters of sterile heparinized saline to flush the catheter. Seventy-five frames of dynamic PET data was yielded over a 120-minute period. Blocking studies involved pretreating monkeys with haloperidol 10 minutes before radioligand administration.

In Figure 7, baseline brain PET/MR images demonstrate [^{18}F]CM304's ability to penetrate the monkey blood-brain barrier. The distribution of [^{18}F]CM304 was shown to accumulate in the cingulate, frontal cortex, occipital cortex, hippocampus, striatum,

cerebellum, and vermis. Also, PET images revealed some accumulation of radioactivity in the monkey skull.

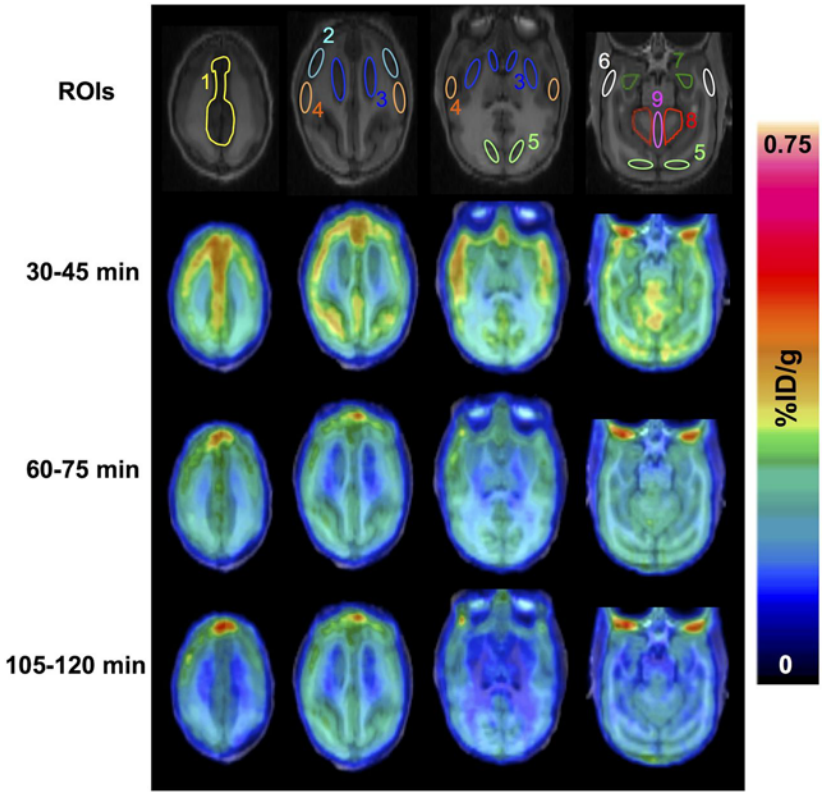

Figure 7: **Monkey brain PET/MR images from baseline dynamic imaging.** Summed axial images are shown for different time intervals after administration of [^{18}F]CM304. Brain regions of interest are shown in MR images and are labeled as (1) cingulate cortex, (2) frontal cortex, (3) striatum, (4) parietal cortex, (5) occipital cortex, (6) temporal cortex, (7) hippocampus, (8) cerebellum, and (9) vermis.
This research was originally published in *JNM*. Author(s). Evaluation of σ-1 James, M. L.; Shen, B.; Nielsen, C. H.; Behera, D.; Buckmaster, C. L.; Mesangeau, C.; Zavaleta, C.; Vuppala, P. K.; Jamalapuram, S.; Avery, B. A.; Lyons, D. M.; McCurdy, C. R.; Biswal, S.; Gambhir, S. S.; Chin, F. T. Evaluation of σ-1 receptor radioligand ^{18}F-FTC-146 in rats and squirrel monkeys using PET. *J Nucl Med*. 2014, 55, 147-153.
© by the Society of Nuclear Medicine and Molecular Imaging, Inc.

Human serum/liver microsome studies were performed to attain information about the potential of [^{18}F]CM304 for eventual clinical translation. The metabolic stability of CM304 was further investigated by determining its half-life in human liver microsomes. CM304 was found to have a longer half-life in human liver microsomes than in mouse and rat liver microsomes that was previously recorded by James and colleagues. The human liver microsome had a half-life of 18.2 ± 3.6 minutes, while the

mouse and rat have half-lives of 4.2 ± 0.6 minutes and 12.6 ± 1.9 minutes, respectively. Imaging sigma-1 receptors via PET could serve as a useful method for detecting sigma-1 receptor-related diseases and monitoring their treatment invasively. Sigma-1 PET imaging could potentially help researchers investigate the in vivo role of sigma-1 receptors in different diseases and enhance the understanding of the pathology/progression of such conditions. In order for PET radiotracers to be successful, a wide range of criteria must be achieved. Ideally, PET radiotracers would possess the following characteristics: high affinity, selectivity for target, ability to penetrate the blood-brain barrier, non-substrate for efflux transporters, lack of troublesome radiometabolites, low non-specific binding, suitable brain pharmacokinetics in relation to radiolabel half-life, amenability to labeling with ^{11}C or ^{18}F at high specific radioactivity, and safe for administration at low tracer dose (Pike, 2008). Several sigma-1 selective PET radioligands have been synthesized; however, none have met all the criteria that were listed above.

Based on the studies of [^{18}F]CM304 in mice, rats, and squirrel monkeys, the radioligand accumulated in regions known to contain high levels of sigma-1 receptors, which suggests that the PET signal specifically binds to sigma-1 receptors in vivo. Another common trend among these animal studies is the accumulation of radioactivity in the skull. Metabolism leading to bone uptake is not desirable and can make quantification of brain signal difficult because of the close proximity of skull to brain and the partial-volume effect of PET. Accuracy of determining sigma-1 receptor levels may be affected (James, 2014). Although the metabolism of [^{18}F]CM304 is a limitation in rodents and nonhuman primates, this does not completely reflect what would occur in

human studies. There have been cases of radiotracers in the literature, such as ^{18}F-SP203, that have defluorinated in nonhuman primates but demonstrated stability in human studies (Brown, 2008). Furthermore, the fact that [^{18}F]CM304 appeared to be more stable in human liver microsomes, compared with mouse and rat liver microsomes, is a good indicator that it might be more stable in humans.

As mentioned in the introduction, sigma-1 receptors may serve a potential role in various neurological diseases, which include addiction, amnesia, chronic pain, depression, Alzheimer's disease, schizophrenia, stroke, retinal neural degeneration, HIV infection, and cancer (Maurice, 2009). Sigma-1 receptors have long been recognized as an endoplasmic reticulum protein. Its involvement in the various diseases has been demonstrated by the molecular biological silencing of the receptor, excluding schizophrenia and HIV infection (Maurice, 2009). The sigma-1 receptor has also been identified as a receptor chaperone whose activity can be activated and deactivated by specific ligands. The mechanism of action of sigma-1 receptors at the molecular level has proven difficult to find by researchers because the sigma-1 receptor does not resemble any of the mammalian proteins as previously mentioned. Several mechanisms of action have been proposed, but the most prominent and the most explored molecular action of sigma-1 receptors centers on the receptor's interaction with voltage-regulated and ligand-gated ion channels, including calcium channels, potassium channels, sodium channels, chloride channels, small conductance calcium-activated potassium channels (SK channels), NMDA receptors and inositol triphosphate (IP3) receptors. According to Maurice and Su, the final output of the action of sigma-1 receptor agonists is to inhibit the voltage-gated ion channels mentioned above, while they potentiate ligand-gated

channels (2009). Sigma-1 receptor antagonists block the inhibition or potentiation induced by sigma-1 agonists.

Studies conducted by Tsai and colleagues have demonstrated that sigma-1 receptors and associated ligands modulate IP3 receptors at the ER membrane. Under physiological conditions, the sigma-1 receptor chaperones the functional IP3 receptor at the endoplasmic reticulum and mitochondrion interface to ensure proper Ca^{2+} signaling from the endoplasmic reticulum to the mitochondria (Tsai, 2009). When cells lose Ca^{2+} homeostasis in the endoplasmic reticulum under pathological conditions, the sigma-1 receptor translocates and counteracts the arising apoptosis. Therefore, the sigma-1 receptor is a receptor chaperone essential for the metabotropic receptor signaling and for the survival against cellular stress (Tsai, 2009).

CHEMISTRY

SN56 and CM304 have extremely similar structures, differing only in the presence of the fluorine at the end of the propyl group. The same benzothiazolone core was used because it has been previously observed by Yous and colleagues that the nature of the surrounding of the tertiary amine nitrogen had an profound impact on sigma-1 affinity. In order to further investigate sigma receptor ligands, the fluoropropyl group was extended to a fluorobutyl group. The insertion of an additional carbon to CM304 was made in hopes of having similar or improved sigma-1 binding compared to CM304 or SN56, without having sigma-2 affinity.

Both SN56 and CM304 were studied in an article written by James and colleagues in 2012. SN56 had demonstrated high selectivity for sigma-1 receptors (>1,000 fold), while CM304 showed even greater selectivity (>145,000 fold) for sigma-1 receptors. Both compounds underwent binding assays, which were performed using brain homogenates. The central nervous system was targeted primarily; however, the liver was also utilized for sigma receptor binding assays. In the rat brain homogenates and the rat liver homogenate binding assays for sigma-1 receptors, SN56 displayed a K_i of 1.7 ± 0.1 nanomolar and $K_i = 1.61 \pm 0.10$ nanomolar, respectively. CM304 demonstrated a K_i of 0.0025 nanomolar in the rat brain homogenate binding assay for sigma-1 receptors and a K_i of 0.96 ± 0.21 nanomolar in the rat liver homogenates. CM304 exhibited greater than 10,000-fold selectivity for sigma-1 receptors compared to all other tested targets. CM304 displayed less than 50% displacement of the radioligand at 10,000 nanomolar screening

concentration and less than 50% displacement for 10 targets at 100 nanomolar screening concentration. These targets include, but are not limited to, α2-adrenoceptors, histamine H_2 receptors, muscarinic M_2 receptors, peripheral muscarinic receptors, neuronal nicotinic receptors, opioid receptors, norepinephrine transporters, calcium L type channels, sodium channels site, and acetylcholine esterase.

To familiarize myself with the procedures for my proposed compound, I performed Schemes 1 and 2 before starting Scheme 3. I got used to using the equipment around the lab and familiarized myself with the reactions that were taking place. In addition, I was synthesizing molecules that the lab needed to be sent off for further investigation. By doing this, I was able to execute the steps confidently and independently after several reactions were performed.

Reagents and starting materials were obtained from commercial suppliers and were used without purification. Precoated silica gel GF Uniplates from Analtech were used for thin-layer chromatography (TLC). Column chromatography was performed on silica gel 60 (Sorbent Technologies).

3-(2-azepan-1-yl)ethyl)-6-(3-methoxypropyl)benzo[d]thiazol-2(3H)-one (**5**) was prepared according to Scheme 1, which is depicted in Figure 8. Commercially available 2-hydroxybenzothiazole (**1**) was reacted with 3-chloroprionyl chloride. The ketone in M1 (**2**) was reduced by using triethylsilane and trifluoroacetic acid. The resulting compound, M2 (**3**), was reacted with 2-(hexamethyleneimino)ethyl chloride hydrochloride to add an azepane functional group to the existing nitrogen, which was an N-alkylation reaction. A

methoxy group replaced the chloride in M3 (**4**) after the compound was reacted with sodium methoxide, giving the final compound.

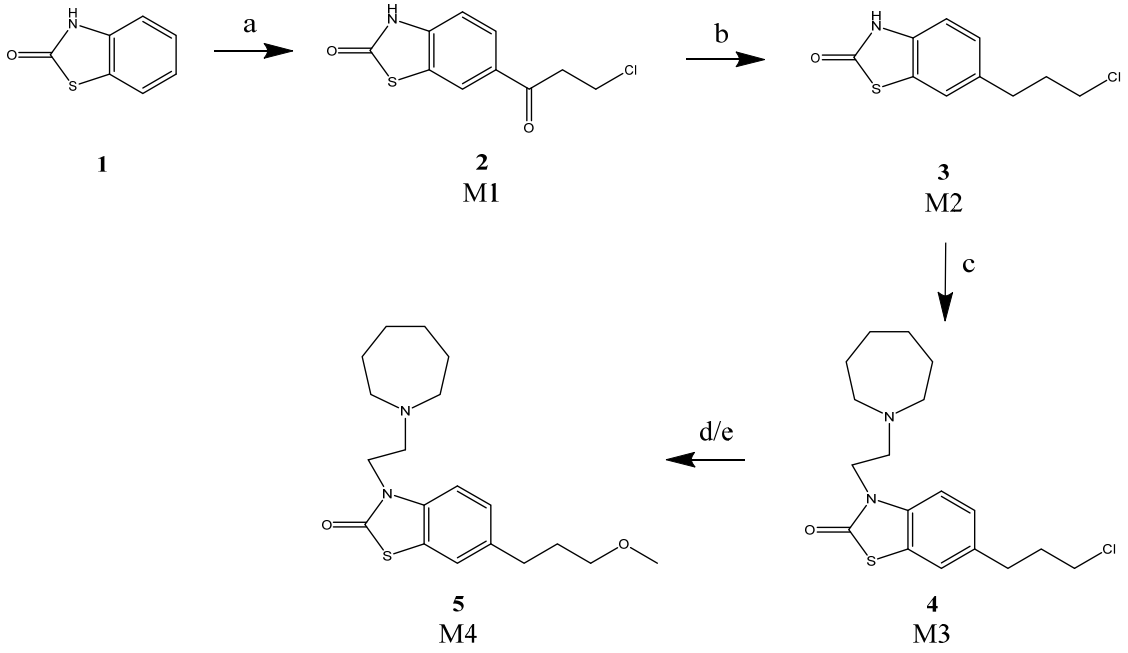

Figure 8: **Scheme 1** Reagents and conditions: (a) 3-chloroprionyl chloride, $AlCl_3$, DMF, 45℃ to 85℃, 4h; (b) Et_3SiH, TFA, rt, 4h; (c) 2-(hexamethyleneimino)ethyl chloride hydrochloride, $NaHCO_3$, DMF, 120℃, 30min (d) $NaOCH_3$, MeOH, 85℃, reflux, overnight (e) $NaOCH_3$, MeOH, KI, 80℃, 1h

The first step in the synthesis is a Friedel-Crafts acylation, which demonstrated in Figure 9. In this specific reaction, 3-chloroprionyl chloride acts as the acyl halide. The first step of an electrophilic aromatic substitution involves the formation of an acylium ion. This occurs when the acyl halide reacts with the aluminum trichloride, $AlCl_3$, a Lewis acid catalyst. The $AlCl_3$ enhances the electrophilicity of the acyl halide by complexing with the chlorine. The chlorine is removed by the Lewis acid catalyst. The acylium ion is then stabilized by resonance, which provides extra stability and prevents the problems associated with the rearrangement of simple carbocation. The next step involves the attack of the acylium ion on the 2-hydroxybenzothiazole as a new electrophile to form one complex. In order for aromaticity to return to the benzene ring of

the 2-hydroxybenzothiazole, a proton leaves. While this is taking place, aluminum tetrachloride, $AlCl_4$, returns to remove a proton from the benzene ring, which allows for the return of the ring's aromaticity. In doing so, the original aluminum trichloride is regenerated, along with hydrochloric acid. As a result, we have the first part of the final product of the reaction, which is a ketone. The addition of water liberates the final product as an acyl benzene.

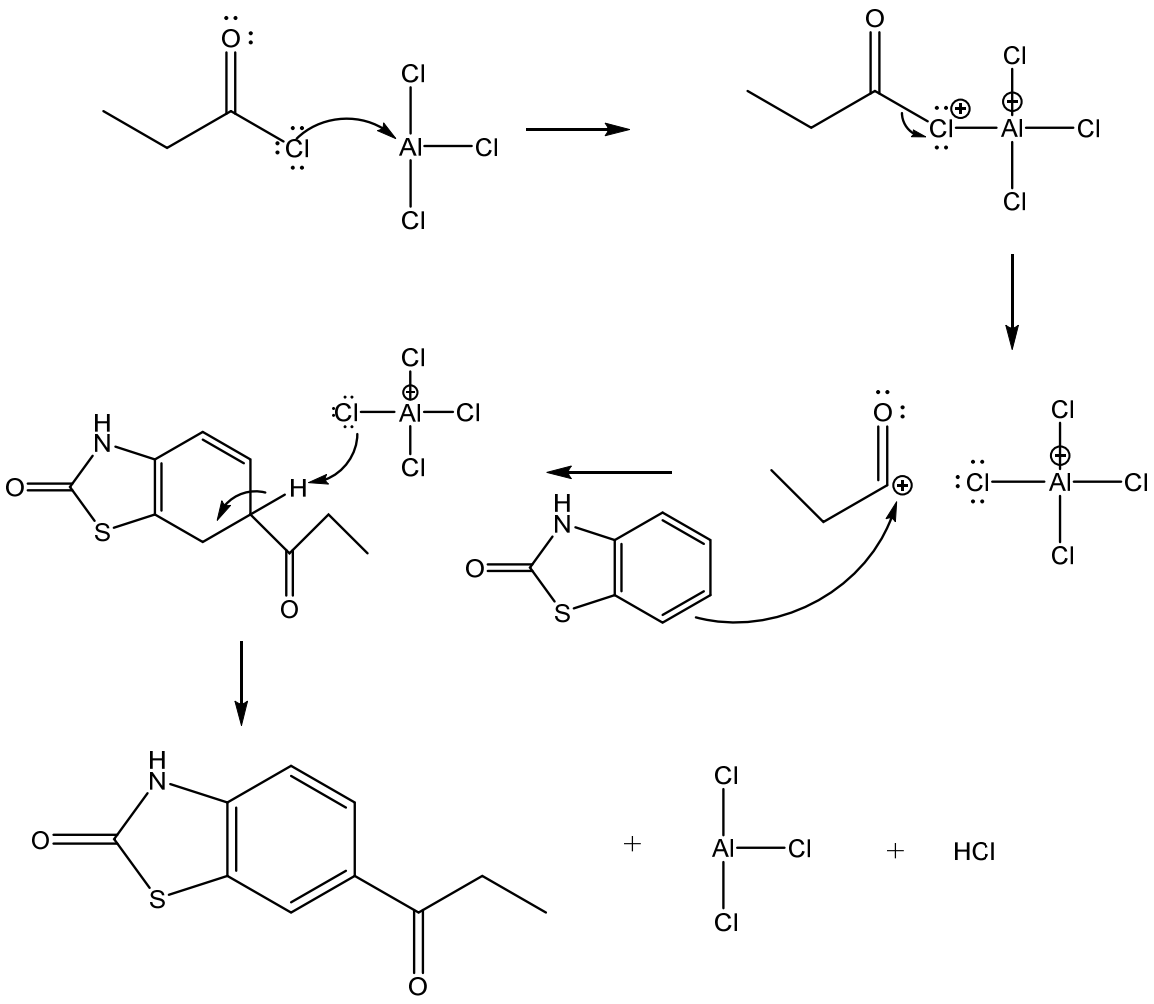

Figure 9: **Friedel-Crafts Acylation Mechanism**

The synthesis of 3-(2-azepan-1-yl)ethyl)-6-(3-hydroxylpropyl)benzo[d]thiazol-2(3H)-one (**4**) is illustrated in Figure 10. M2 (**1**) had been previously synthesized using the first step from Scheme 1. The chlorine of the propyl chain in M2 (**1**) was replaced with benzoic acid during a benzoate-ester reaction. The azepane group was linked to the existing nitrogen of M5 (**2**). The resulting compound, M6 (**3**), was reduced using a combination of sodium hydroxide and water.

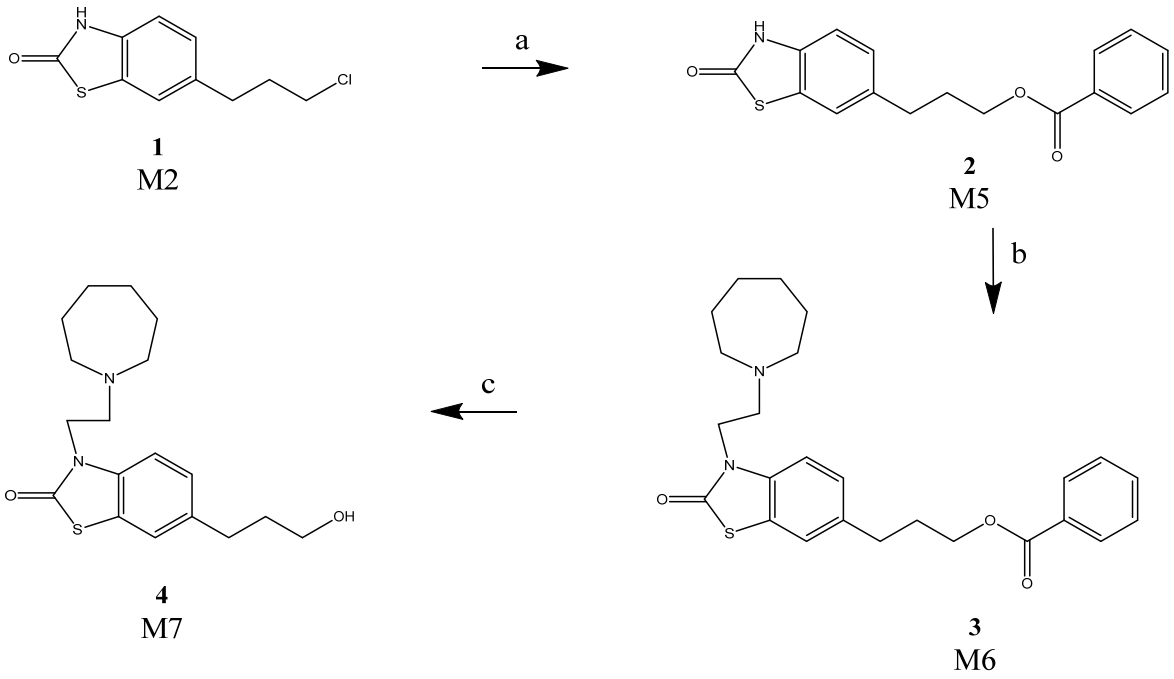

Figure 10: **Scheme 2** Reagents and conditions: (a) K_2CO_3, benzoic acid, DMF, 110℃, 4h (b) K_2CO_3, 2-(hexamethyleneimino)ethyl chloride hydrochloride, DMF, 65℃, 4h (c) MeOH, NaOH, H_2O, 90℃, 1h

The schematic for the synthesis of the modified 2(3H)-benzothiazolone is depicted in Figure 11. The scheme followed a combination of Scheme 1 and Scheme 2 with a few exceptions. 4-chlorobutyryl chloride was used instead of 3-chloroprionyl chloride, and additional steps were taken to reach the final product. After the hydrolysis of 4-(3-(2-azepan-1-yl)ethyl)-2-oxo-2,3-dihydrobenzo[d]thiazol-6-yl)butyryl benzoate (**5**) using sodium hydroxide and water, the resulting compound was reacted with p-

toluenesulfonyl chloride to give M13 (**7**). M13 was reacted with tetrabutylammonium fluoride to replace the tosyl group with a fluorine to yield M14 (**8**).

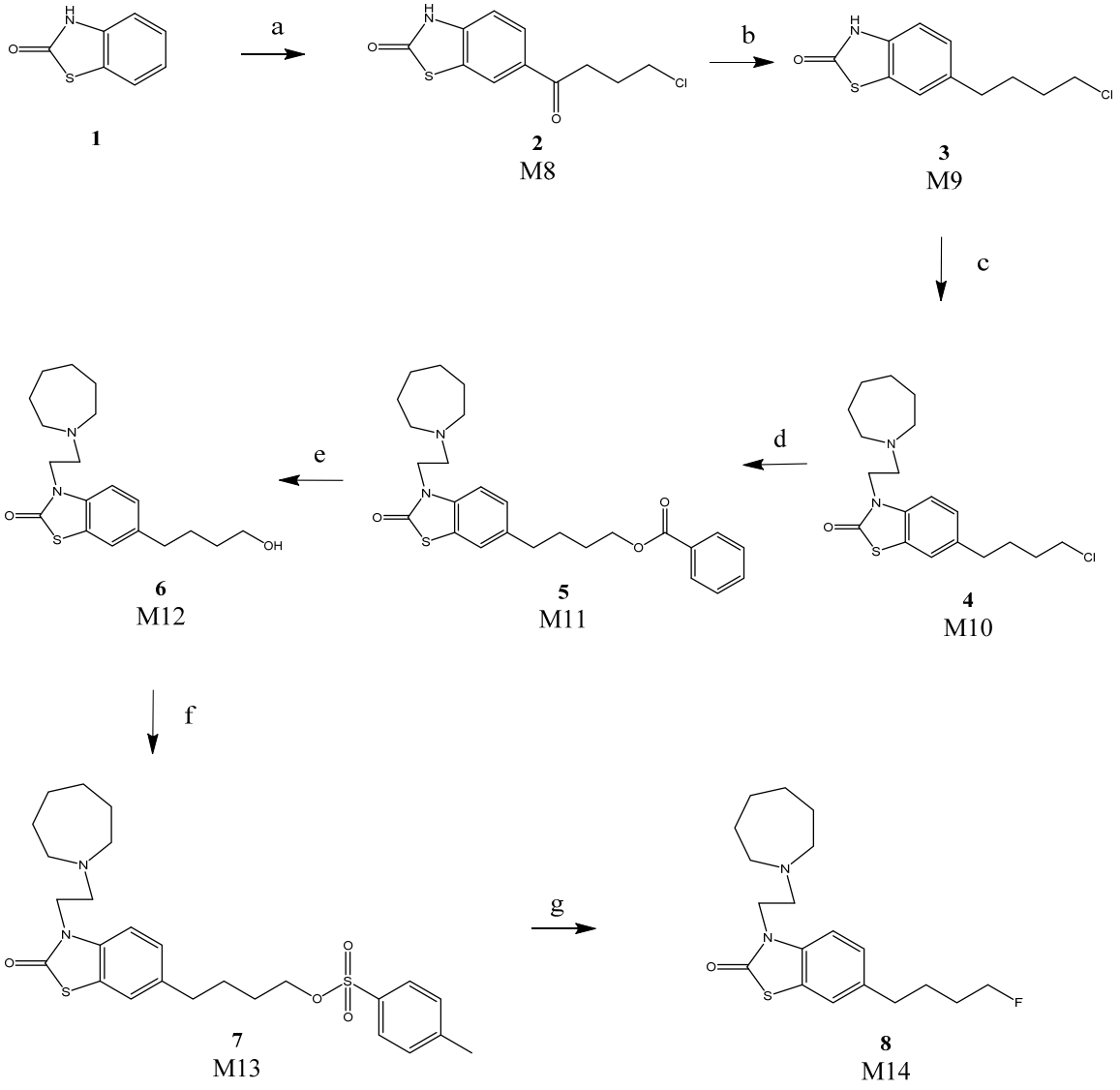

Figure 11: **Scheme 3** Reagents and conditions: (a) 4-chlorobutyryl chloride, $AlCl_3$, DMF, 45℃ to 85℃, 6h; (b) Et_3SiH, TFA, rt, 4h; (c) 2-(hexamethyleneimino)ethyl chloride hydrochloride, $NaHCO_3$, DMF, 120℃, 30min (d) K_2CO_3, benzoic acid, DMF, 110℃, 2h (e) MeOH, NaOH, H_2O, 90℃, 1h (f) p-toluenesulfonyl chloride, DCM, triethylamine, rt, 8h (g) TBAF/THF, 60℃, 4h

An electron pushing mechanism for Scheme 3 was created to further illustrate how the reactions were taking place. This is shown in Figure 12.

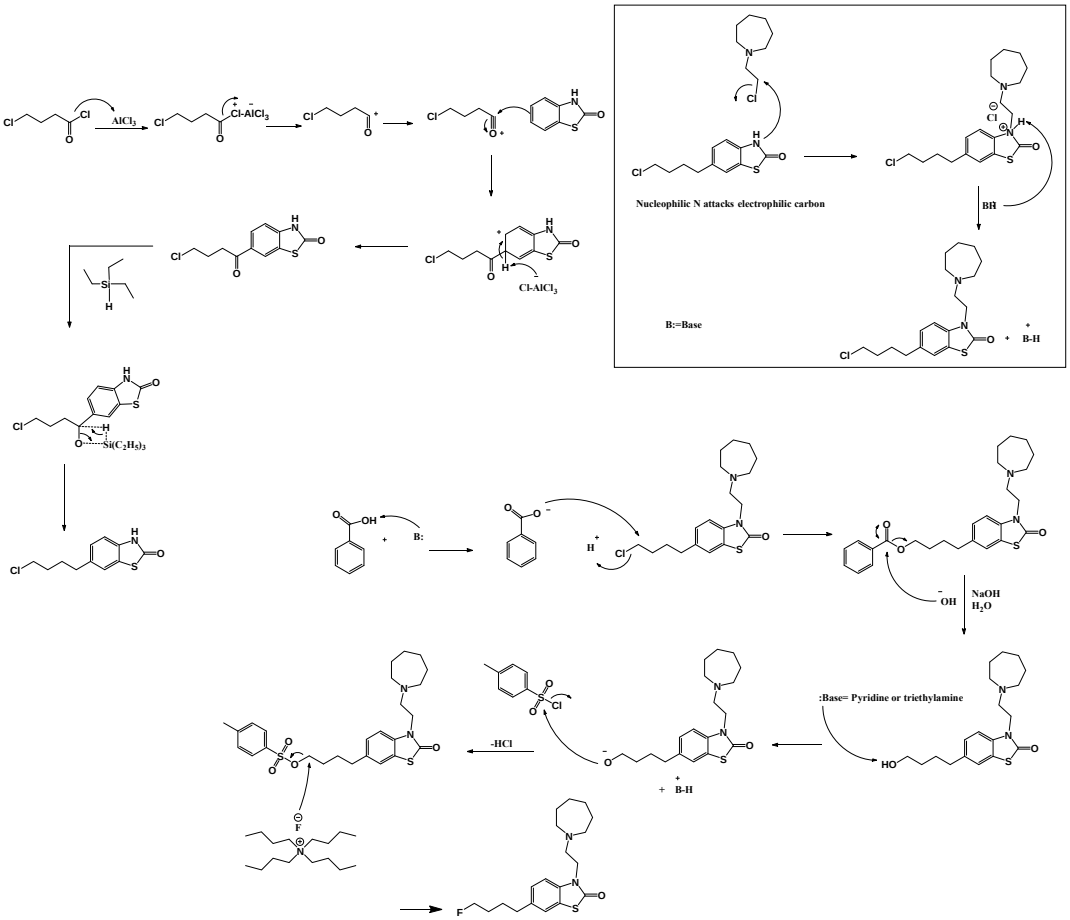

Figure 12: **Electron Pushing Mechanism**

DISCUSSION AND FUTURE DIRECTIONS

Findings from James and colleagues in 2012 demonstrated that the small structural modification made to SN56 in order to create CM304 led to an improvement in affinity and selectivity for sigma-1 receptors. Both the affinity and selectivity of CM304 are higher than values reported for most other known sigma-1 receptor ligands, such as [^{11}C]SA4503, [^{18}F]FM-SA4503, [^{18}F]FPS, and [^{18}F]SFE (see Figure 13).

Available PET Tracers for Sigma-1

S1R PET Tracer	S1R K_i (nM)	S2R/S1R	PET Studies			Comments
			Rodent	Monkey	Human	
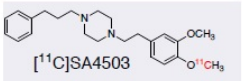 [^{11}C]SA4503	4.4	242	✓	✓	✓	- Only S1R tracer being used in clinical studies - Non-specific binding - Irreversible binding
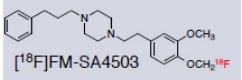 [^{18}F]FM-SA4503	6.4	250	✓ (ex vivo BIO-D)	✓	✗	- Bone accumulation - Irreversible binding
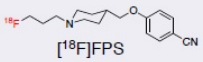 [^{18}F]FPS	0.5	288	✓ (ex vivo BIO-D)	✓	✓	- Irreversible binding in humans - Some bone uptake
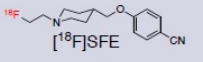 [^{18}F]SFE	5.0	72	✓ (ex vivo BIO-D)	✗	✗	- Toxicity issues in dogs - Selectivity? - No displacement - No PET imaging studies
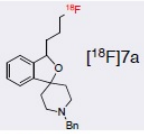 [^{18}F]7a	1.4	>600	✓ (ex vivo BIO-D)	✗	✗	- Bone accumulation - Very early stages
CM304	0.0025	>145,000				

Figure 13: **Available PET Tracers for Sigma-1**

In the first scheme, a methoxy group was added to the end of the propyl chain in SN56, resulting in 3-(2-azepan-1-yl)ethyl)-6-(3-methoxypropyl)benzo[d]thiazol-2(3H)-one (M4). The purpose of this synthesis was to create a non-radioactive compound, which is often referred to as a "cold" compound, that could be used as a PET ligand that

ultimately expresses similar or improved sigma-1 binding compared to CM304 or SN56 without having sigma-2 affinity. The methoxy group mimics the number of atoms in the molecule's tail. Therefore, the addition of the methoxy group should improve sigma-1 affinity; however, the effects of the oxygen are unknown. The methyl of the methoxy group can be labeled with a ^{11}C, which would provide an alternative to fluorine-based imaging. The oxygen of the methoxy group should behave similarly to fluorine because it should be able to accept hydrogen bonds due to the oxygen's partial negative charge. The oxygen also allows researchers to synthesize isotopes more easily. Because the structure of M4 is similar to SN56, predictions can be made based off the previous studies on SN56: M4 is expected to have relatively high affinity for sigma-1 receptors.

With a minor addition of a carbon on the propyl group of CM304, one could suspect M14 to possess similar sigma-1 binding properties without sigma-2 affinity. The goal of synthesizing M14 was to create a compound that have similar, possibly even better, binding to sigma-1 compared to CM304 or SN56. Based on previous studies, evidence suggests that there are several properties of M14 that would make it an ideal PET radioligand (Yous, 2005). In an article by Yous and colleagues, compounds similar to SN56, CM304, and M14 were synthesized, and the affinities for sigma-1 and sigma-2 receptors were evaluated. The same modifications were done to these similar compounds; therefore, the same patterns are expected. Three specific modifications that were displayed in this study to the molecules includes the addition of a methyl group to the propyl chain, the inclusion of a seven-membered rings, and the addition of the fluorine. All of these modifications were shown to improve sigma-1 receptor affinity; however, an accurate assessment cannot be made.

Both compounds (M4 and M14) are expected to have relatively high affinity for sigma-1 receptors because of the presence of the benzothiazole. The large increase in affinity in CM304 to sigma-1 receptors may be due to the interaction with one or more amino acid residues in the sigma-1 protein when engaged, which should be present with these compounds.

Shen and colleagues established a rat-model of neuropathic pain and nerve injury called the spared nerve injury (SNI) model. In this model, scientists carefully injury the tibial and common peroneal branches but spared the sural branch of the left sciatic nerve. After four weeks, pain behavioral response was tested using Von Frey filaments to confirm development of pain in SNI rats and the lack of pain in sham-operated (surgical wound but no nerve injury) and control rats (uninjured rats with no surgery or wound). Von Frey filament tests indicated the development of allodynia (pain produced by an otherwise non-painful stimulus) observed in the left hind paws of the SNI rats. The SNI rats exhibited decreased paw withdrawal thresholds, indicating pain, in the injured left hind limb compared to levels observed for the uninjured right side of SNI rats, sham-operated rats, and control rats. [^{18}F]CM304 accumulated in the injured nerve compared to the uninjured right sciatic nerve of SNI rats as well as the nerves of the sham-operated rats and control rates. The left injured nerves showed higher signals during autoradiography. [^{18}F]CM304 was able to detect the site of nerve injury in SNI rats via PET/MR imaging and ex vivo autoradiography. The specific binding of [^{18}F]CM304 to sigma-1 receptor is further supported by the blocking studies with haloperidol. The relationship between pain behavior (determined via Von Frey tests) and the normalized PET signal in sciatic nerves, Shen found a strong negative correlation between the two.

That is, a lower Von Frey threshold denotes greater pain, which correlated with increased PET signal.

Shen and colleagues' study established four significant findings: (1) [^{18}F]CM304-PET/MRI enabled detection of peripheral nerve injury in a rat model of neuropathic pain; (2) the normalized PET in injured sciatic nerves correlated with pain sensitivity and severity; (3) the site of nerve injury was shown to contain increased expression of sigma-1 receptors; and (4) there was significant correlation between the levels of sigma-1 receptors and the uptake of [^{18}F]CM304 (2015).

As demonstrated by Shen and colleagues, specific binding of [^{18}F]CM304 to sigma-1 receptors in site of nerve injury suggest that increased sigma-1 receptor expression is associated with pain generation and nerve injury. The strong correlation between PET signal and pain levels indicates the possibility of providing accurate, non-invasive estimates about pain severity. Furthermore, [^{18}F]CM304 could provide information about the precise location and magnitude of sigma-1 receptor expression as a potential pain biomarker. The imaging approach of [^{18}F]CM304 in combination of PET with MRI satisfies the need for sensitivity and specificity to diagnose nerve injury without being invasive. Sigma-1 receptor-PET imaging as a non-invasive biomarker of nerve injury and inflammation could significantly impact pain therapeutics.

Future work with these compounds include tagging the precursor of M14, of 4-(3-(2-(azepan-1-yl)ethyl)-2-oxo-2,3-dihydrobenzo[d]thiazol-6-yl)butyl 4-methylbenzenesulfonate, with a radioactive fluorine. The synthesis of [^{18}F]M14 could be performed by the Molecule Imaging Program at Stanford Department of Radiology since

other compounds have previously been sent here. The strategy for generating [^{18}F]M14 would involve the preparation of its tosylate precursor, M13, and its subsequent radiolabeling with fluorine-18. Fluorine-18 radiolabelling could be accomplished by reacting its tosylate precursor with cyclotron-produced ^{18}F-fluorine as a Kryptofix-222/K^+/[^{18}F]F^- complex in DMSO at 150^{o}C for 15 minutes (James 2012). This would allow researchers to test the compound in animals with PET.

Further investigation involving sigma-1 receptors involves synthesizing selective sigma-1 receptor PET radiotracers. CM304 has looked very promising as a potential PET radioligand. Compared to other available sigma-1 receptor PET radiotracers, [^{18}F]CM304 appears to have several key advantages, including its picomolar affinity for sigma-1 receptors; high brain uptake in mouse, rat, and monkey; favorable kinetic profile; and the fact that it has the highest selectivity for sigma-1 receptors over sigma-2 receptors of any sigma-1 receptor radiotracer (James, 2014). By using CM304 as the lead compound, we would expect M14 to exert similar properties because the same modification was seen from the reaction of SN56 to CM304.

CONCLUSIONS

Benzothiazole-based compounds were synthesized to serve as possible selective sigma-1 receptor PET radioligands. Currently, no biological data have been collected on these compounds. Therefore, the binding affinities and selectivity for sigma-1 receptors are unknown. However, predictions about the general properties of the compounds synthesized can be made. Each of the compounds is expected to have relatively high selectivity and binding to sigma-1 receptors and lack of sigma-2 affinity due to the compound's similar structure to SN56 and CM304. Further studies will be conducted to assess their selectivity and affinity toward sigma-1 receptors and their efficacy of becoming a radioligand for PET imaging.

EXPERIMENTAL

Synthesis of 3-(2-azepan-1-yl)ethyl)-6-(3-methoxypropyl)benzo[d]thiazol-2(3H)-one.

6-(3-chloropropanoyl)benzo[d]thiazol-2(3H)-one (M1). Aluminum chloride (53.3 grams, 400 millimoles) was first added to an Erlenmeyer flask. Next, dimethylformamide (8.6 milliliters, 115 millimoles) was slowly added under vigorous stirring. After 15 minutes of stirring, 2-hydroxybenzothiazole (6.04 grams, 40 millimoles) was added, and the mixture was heated at 45°C. After 15 minutes, 3-chloropropionyl chloride was added and the reaction mixture was slowly raised to 85°C and stirred for 3 hours. Once starting material was no longer present in the reaction, the hot mixture was carefully poured onto ice. 150 milliliters of 3N hydrochloric acid was added to neutralize the reaction, and the mixture was stirred for 30 more minutes. The mixture was filtered by vacuum filtration, and the crude product was collected and dissolved in a mixture of ethyl acetate and water. The layers were then separated, and the organic layer was washed with brine and dried with sodium sulfate. The organic layer was transferred to a round bottom flask, and the solvent was removed in vacuo. The residue was recrystallized from toluene/dioxane to give 5.50 grams (55.5%) of 6-(3-chloropropanoyl)benzo[d]thiazol-2(3H)-one as an orange solid.

6-(3-chloropropyl)benzo[d]thiazol-2(3H)-one (M2). M1 (5.50 grams, 22.75 millimoles) was added to a dry round bottom flask, and 30 milliliters of trifluoroacetic acid was added. To the stirred solution, triethylsilane (8.36 mL, 52.32 millimoles) was added. The

reaction mixture was stirred for 4 hours at room temperature. The solvent was carefully removed in vacuo, and the residue was purified by column chromatography using a gradient of ethyl acetate and hexane to give 1.8776 grams (36.2%) of 6-(3-chloropropyl)benzo[d]thiazol-2(3H)-one as a white crystalline solid.

3-(2-(azepan-1-yl)ethyl)-6-(3-chloropropyl)benzo[d]thiazol-2(3H)-one (M3). In a dry round bottom flask, M2 (1.8776 grams, 8.246 millimoles) was dissolved in 25 milliliters of dimethylformamide. 2-(Hexamethyleneimino)ethyl chloride hydrochloride (6.5351 grams, 32.98 millimoles) was added and the reaction mixture was heated to 120°C. Then sodium bicarbonate was slowly added and the reaction was left for 30 minutes. The mixture was poured into water and extracted with ethyl acetate three times. The layers were separated, and the organic layer was washed with brine and dried with sodium sulfate. The organic layer was then transferred to a round bottom flask, and the solvent was removed in vacuo. The residue was purified with column chromatography and resulted in 1.10 grams (37.8%) of 3-(2-(azepan-1-yl)ethyl)-6-(3-chloropropyl)benzo[d]thiazol-2(3H)-one as a white solid.

3-(2-azepan-1-yl)ethyl)-6-(3-methoxypropyl)benzo[d]thiazol-2(3H)-one (M4). M3 (1.0 grams, 2.83 millimoles) was dissolved in 10 milliliters of methanol in a dry round bottom flask. Sodium methoxide (660 milligrams, 1.72 millimoles) was then added to the reaction mixture. The reaction was heated under reflux at 85^{o}C until starting material was no longer present. The solvent was removed in vacuo, and the residue was subjected to purification by silica gel column chromatography to afford approximately 150 milligrams (15.2%) of 3-(2-azepan-1-yl)ethyl)-6-(3-methoxypropyl)benzo[d]thiazol-2(3H)-one as a white solid.

Synthesis of 3-(2-azepan-1-yl)ethyl)-6-(3-hydroxylpropyl)benzo[d]thiazol-2(3H)-one.

3-(2-oxo-2,3-dihydrobenzo[d]thiazol-6-yl)propyl benzoate (M5). About 20 milliliters of dimethylformamide was used to dissolve M2 (1.0 grams, 4.39 millimoles) in a round bottom flask. Under mechanical stirring, potassium carbonate (1.517 grams, 10.979 millimoles) and benzoic acid (2.682 grams, 21.95 millimoles) were added to the reaction mixture. The reaction was heated to 110^{o}C. After 4 hours, the reaction was stopped and left to cool down. The mixture was then poured into 200 milliliters of water and extracted with ethyl acetate. The solvent was removed in vacuo, and the residue was purified through a column chromatograph using ethyl acetate and hexane as the eluent to yield 1.221 grams (86.7%) of 3-(2-oxo-2,3-dihydrobenzo[d]thiazol-6-yl)propyl benzoate as a white solid.

3-(3-(2-(azepan-1-yl)ethyl)-2-oxo-2,3-dihydrobenzo[d]thiazol-6-yl)propyl benzoate (M6). In a dry round bottom flask, M5 (1.221 grams, 3.8986 millimoles) was dissolved in about 20 milliliters of dimethylformamide. Potassium carbonate (1.6164 grams, 11.6958 millimoles) and 2-(hexamethyleneimino)ethyl chloride hydrochloride was added to the solution under mechanical stirring. The reaction mixture was heated at 65^{o}C for 4 hours. Once the starting material was gone, the reaction was cooled. The mixture was then poured into 200 milliliters of water and extracted with ethyl acetate. The organic layer was washed with brine and dried with sodium sulfate. The solvent was removed in vacuo, and the residue was chromatographed on a silica gel column, resulting in 1.3029 grams (76.3%) of 3-(3-(2-(azepan-1-yl)ethyl)-2-oxo-2,3-dihydrobenzo[d]thiazol-6-yl)propyl benzoate as a white solid.

3-(2-azepan-1-yl)ethyl)-6-(3-hydroxylpropyl)benzo[d]thiazol-2(3H)-one (M7). M6 (1.10 grams, 2.5117 millimoles) was dissolved in 15 milliliters of methanol. The solution was then added to of a solution of sodium hydroxide (0.251 grams, 6.275 millimoles) in 15 milliliters of distilled water. The mixture was heated at 90^{o}C for 1 hour, concentrated in vacuo, poured into 1N hydrochloric acid, and extracted with ethyl acetate. The pH of the aqueous layer was adjusted to 10 with potassium carbonate, and the mixture was extracted with ethyl acetate. The organic layer was dried and transferred into a round bottom flask to evaporate the solvent. The residue was purified by silica gel column chromatography using methanol and dichloromethane as the eluent to give 330 milligrams (39.3%) of 3-(2-azepan-1-yl)ethyl)-6-(3-hydroxylpropyl)benzo[d]thiazol-2(3H)-one.

Synthesis of 3-(2-azepan-1-yl)ethyl)-6-(4-fluorobutyl)benzo[d]thiazol-2(3H)-one.

6-(4-Chlorobutanoyl)benzo[d]thiazol-2(3H)-one (M8). Aluminum chloride (17.628 grams, 132.3 millimoles) was first added to an Erlenmeyer flask. Next, dimethylformamide (3 milliliters, 40 millimoles) was slowly added under vigorous stirring. After 15 minutes of stirring, 2-hydroxybenzothiazole (2.0 grams, 13.23 millimoles) was added, and the mixture was heated at 45°C. After 15 minutes, 4-chlorobutyryl chloride (2.224 milliliters, 19.845 millimoles) was added. After 1 hour, the reaction mixture was slowly raised to 85°C and stirred for 4 hours. Once starting material was no longer present in the reaction, the hot mixture was carefully poured onto ice. 150 milliliters of 3N hydrochloric acid was added to neutralize the reaction, and the mixture was stirred for 30 more minutes. Once the reaction mixture came into contact with the ice, an exothermic reaction should have taken place; however, no heat was produced. The

product that was synthesized became a sticky residue. Filtration was supposed to take place like in Scheme 1, but this step was skipped because the product remained in a clump. Instead, the sticky product was then dissolved in ethyl acetate. Water was added, and the layers were separated. The organic layer was washed with brine and dried with sodium sulfate. The organic layer was transferred to a round bottom flask, and the solvent was removed in vacuo. The residue was purified with a silica gel column chromatography using a ethyl acetate and hexane eluent to afford 900 milligrams (26.7%) of 6-(4- Chlorobutanoyl)benzo[d]thiazol-2(3H)-one. ^{1}H NMR (400 MHz, Chloroform-d) δ 10.67 (s, 1H), 8.05 (d, *J* = 8.1 Hz, 1H), 7.92 (dd, *J* = 8.4, 1.7 Hz, 1H), 7.28 – 7.23 (m, 1H), 3.68 (t, *J* = 6.1 Hz, 2H), 3.17 (t, *J* = 7.0 Hz, 2H), 2.23 (p, *J* = 6.7 Hz, 2H).^{13}C NMR (101 MHz, $CDCl_3$) δ 197.28, 173.11, 139.45, 132.16, 127.13, 124.51, 122.84, 111.56, 44.61, 35.13, 26.77. MS (ESI) *m/z* (M^+ + Na) 278

6-(4-Chlorobutyl)benzo-[d]thiazol-2(3H)-one (M9). M8 (0.900 grams, 3.529 millimoles) was transferred to a dry round bottom flask, and 5 milliliters of trifluoroacetic acid was added. To the stirred solution, triethylsilane (1.368 milliliters, 8.1167 millimoles) was added. The reaction mixture was stirred for 3 hours at room temperature. The solvent was carefully removed in vacuo, and the residue was purified by column chromatography using a gradient of ethyl acetate and hexane to give 409 milligrams (48.3%) of 6-(4-chlorobutyl)benzo[d]thiazol-2(3H)-one as a white crystalline solid. Used without further purification.

3-(2-azepan-1-yl)ethyl)-6-(4-chlorobutyl)benzo[d]thiazol-2(3H)-one (M10). In a dry round bottom flask, M9 (0.6482 grams, 2.7 millimoles) was dissolved in 25 milliliters of dimethylformamide. 2-(Hexamethyleneimino)ethyl chloride hydrochloride (2.141 grams,

10.8 millimoles) was added and the reaction mixture was heated to 120°C. Then sodium bicarbonate (2.271 grams, 27 millimoles) was slowly added and the reaction was left for 30 minutes. The mixture was poured into water and extracted with ethyl acetate. The layers were separated, and the organic layer was washed with brine and dried with sodium sulfate. The organic layer was then transferred to a round bottom flask, and the solvent was removed in vacuo. The residue was purified with column chromatography and resulted in 0.9425 grams (95.6%) of 3-(2-azepan-1-yl)ethyl)-6-(4-chlorobutyl)benzo[d]thiazol-2(3H)-one as a white solid. ^{1}H NMR (400 MHz, Chloroform-d) δ 7.23 (s, 1H), 7.11 (dd, *J* = 8.3, 1.8 Hz, 1H), 7.02 (d, *J* = 8.2 Hz, 1H), 4.05 – 3.99 (m, 2H), 3.54 (t, *J* = 6.0 Hz, 2H), 2.84 – 2.78 (m, 2H), 2.74 (t, *J* = 5.5 Hz, 4H), 2.66 (q, *J* = 7.3, 6.2 Hz, 3H), 1.78 (dd, *J* = 7.9, 4.2 Hz, 4H), 1.63 (dd, *J* = 9.5, 4.9 Hz, 5H). ^{13}C NMR (101 MHz, $CDCl_3$) δ 169.77, 136.87, 135.37, 126.42, 122.78, 122.23, 110.54, 55.70, 54.68, 44.77, 41.17, 34.66, 31.90, 28.72, 28.17, 26.90. MS (ESI) *m/z* (M^+ + H) 367.5

4-(3-(2-azepan-1-yl)ethyl)-2-oxo-2,3-dihydrobenzo[d]thiazol-6-yl)butyl benzoate (M11). Approximately 25 milliliters of dimethylformamide was added to M10 (0.8837 grams, 2.421 millimoles) in a round bottom flask. Potassium carbonate (0.8365 grams, 6.0525 millimoles) and benzoic acid (1.478 grams, 12.105 millimoles) were then added to the solution. The reaction was heated to 110^{o}C and stirred for 2 hours. The mixture was poured into distilled water and extracted with ethyl acetate. The layers were separated, and the organic layer was washed with brine and dried with sodium sulfate. The solvent was evaporated in vacuo. The reaction resulted in 880 milligrams (80.8%) of 4-(3-(2-azepan-1-yl)ethyl)-2-oxo-2,3-dihydrobenzo[d]thiazol-6-yl)butyl benzoate as a

pale yellow viscous oil. ^{1}H NMR (400 MHz, Chloroform-d) δ 8.08 – 8.01 (m, 2H), 7.56 (t, *J* = 7.4 Hz, 1H), 7.45 (q, *J* = 7.7, 6.9 Hz, 2H), 7.27 (s, 1H), 7.13 (q, *J* = 8.3 Hz, 2H), 4.35 (t, *J* = 5.6 Hz, 2H), 4.11 (t, *J* = 7.4 Hz, 2H), 2.86 (dt, *J* = 19.6, 6.1 Hz, 7H), 2.72 (d, *J* = 7.2 Hz, 2H), 1.80 (dt, *J* = 7.7, 3.7 Hz, 3H), 1.68 (dd, *J* = 9.7, 4.9 Hz, 4H), 1.64 – 1.58 (m, 4H). ^{13}C NMR (101 MHz, $CDCl_3$) δ 169.85, 166.60, 137.16, 135.20, 132.88, 130.34, 129.51, 128.34, 126.61, 122.74, 122.27, 110.66, 64.67, 55.52, 54.35, 40.67, 35.04, 28.21, 27.98, 27.51, 26.91. MS (ESI) *m/z* (M^+ + H) 453.56

3-(2-azepan-1-yl)ethyl)-6-(4-hydroxybutyl)benzo[d]thiazol-2(3H)-one (M12). M11 (0.850 grams, 1.890 millimoles) was dissolved in 15 milliliters of methanol. The solution was added to sodium hydroxide (0.184 grams, 4.720 millimoles) that was in 15 milliliters of water. The mixture was heated at 90^{o}C for 1 hour and concentrated in vacuo. The mixture was poured into 1N hydrochloric acid and extracted with ethyl acetate. The pH of the aqueous layer was adjusted to 10 with potassium carbonate, and the mixture was extracted with ethyl acetate. The organic layer was dried with sodium sulfate, and the solvent was evaporated in vacuo. The reaction resulted in 430 milligrams (65%) of 3-(2-azepan-1-yl)ethyl)-6-(4-hydroxybutyl)benzo[d]thiazol-2(3H)-one. ^{1}H NMR (400 MHz, Chloroform-d) δ 7.24 (d, *J* = 1.6 Hz, 1H), 7.15 – 7.07 (m, 2H), 4.14 – 4.05 (m, 2H), 3.66 (t, *J* = 6.4 Hz, 2H), 2.90 – 2.79 (m, 6H), 2.66 (t, *J* = 7.5 Hz, 2H), 1.72 – 1.55 (m, 13H). ^{13}C NMR (101 MHz, $CDCl_3$) δ 169.90, 137.57, 135.04, 126.63, 122.61, 122.28, 110.60, 77.36, 77.04, 76.72, 62.56, 55.61, 54.42, 40.65, 35.20, 32.13, 27.76, 27.55, 26.85. MS (ESI) *m/z* (M^+ + H) 349.54

4-(3-(2-(azepan-1-yl)ethyl)-2-oxo-2,3-dihydrobenzo[d]thiazol-6-yl)butyl 4-methylbenzenesulfonate (M13). A solution of M12 (0.200 grams, 0.572 millimoles) in

triethylamine (0.16 milliliters, 1.144 millimoles) and 5 milliliters of dichloromethane was made. A solution of *p*-toluenesulfonyl chloride (0.120 grams, 0.6292 millimoles) in dichloromethane (5 milliliters) was added to the existing mixture. The mixture was stirred for 8 hours at room temperature. The solvent was evaporated in vacuo. The residue was purified using silica gel column chromatography employing 2% methanol and dichloromethane as the mobile phase to obtain 110 milligrams (38.1%) of 4-(3-(2-(azepan-1-yl)ethyl)-2-oxo-2,3-dihydrobenzo[d]thiazol-6-yl)butyl 4-methylbenzenesulfonate as a yellow viscous oil. ^{1}H NMR (400 MHz, Chloroform-d) δ 7.81 – 7.74 (m, 2H), 7.34 (d, *J* = 7.9 Hz, 2H), 7.16 (d, *J* = 1.6 Hz, 1H), 7.09 – 7.01 (m, 2H), 4.04 (dd, *J* = 8.4, 6.4 Hz, 4H), 2.84 (dd, *J* = 8.5, 6.1 Hz, 2H), 2.79 – 2.75 (m, 4H), 2.59 (t, *J* = 6.9 Hz, 2H), 2.44 (s, 3H), 1.68 – 1.56 (m, 12H). ^{13}C NMR (101 MHz, $CDCl_3$) δ 169.76, 144.75, 136.64, 135.34, 133.09, 129.83, 127.84, 126.46, 122.75, 122.21, 110.58, 77.36, 77.04, 76.73, 70.22, 55.68, 54.61, 41.04, 34.65, 28.23, 28.00, 27.31, 26.89, 21.63. MS (ESI) *m/z* (M^+ + H) 503.56

3-(2-azepan-1-yl)ethyl)-6-(4-fluorobutyl)benzo[d]thiazol-2(3H)-one (M14). A solution of tetrabutylammonium fluoride (TBAF) in THF (1M/THF, 0.280 milliliters, 0.287 millimoles) was added to a solution of M13 (100 milligrams, 0.199 millimoles) in THF (10 milliliters). The reaction mixture was heated to 60^{o}C and stirred for 4 hours. The solution was concentrated, and the residue was dissolved with 20 milliliters of ethyl acetate. The solution was washed with 10% aqueous sodium bicarbonate solution, water, and brine. The organic layers were dried with sodium sulfate and concentrated in vacuo. The residue was purified by silica gel column chromatography using methanol and chloroform as the eluent to obtain 30 milligrams (43.1%) of 3-(2-azepan-1-yl)ethyl)-6-(4-

fluorobutyl)benzo[d]thiazol-2(3H)-one as a yellow viscous oil. ^{1}H NMR (400 MHz, Methanol-d4) δ 7.33 (s, 1H), 7.17 (t, *J* = 6.5 Hz, 2H), 4.47 (d, *J* = 5.3 Hz, 1H), 4.36 (t, *J* = 5.7 Hz, 1H), 4.05 (t, *J* = 7.1 Hz, 2H), 2.94 – 2.57 (m, 8H), 1.77 – 1.51 (m, 12H). ^{13}C NMR (101 MHz, MeOD) δ 170.31, 137.68, 135.06, 126.63, 122.20, 122.08, 110.74, 84.11, 82.48, 55.35, 54.33, 48.28, 48.07, 47.85, 47.64, 47.43, 47.21, 47.00, 40.17, 34.58, 29.74, 29.55, 29.41, 27.29, 27.12, 27.07, 26.50. MS (ESI) *m/z* (M^+ + H) 351.68

REFERENCES

1. Bowen, W. D. σ receptors: recent advances and new clinical potentials. *Pharm. Acta. Helv.* 2000, 74, 211-218.
2. Brown, A. K.; Kimura, Y.; Zoghbi, S. S.; Siméon, F. G.; Liow, J.; Kreisl, W. C.; Taku, A.; Fujita, M.; Pike, V. W.; Innis, R. B. Metabotropic glutamate subtype 5 receptors are quantified in the human brain with novel radioligand for PET. *J Nucl Med*. 2008, 49, 2042-2048.
3. Chapter 12: reactions of arenes, electrophilic aromatic substitution [Internet]. Calgary, Canada: University of Calgary [cited 2014 Dec 15]. Available from: http://www.chem.ucalgary.ca/courses/350/Carey5th/Ch12/ch12-7.html.
4. Cobos, E. J.; Entrena, J. M.; Nieto, F. R.; Cendan, C. M.; Del Pozo, E. Pharmacology and therapeutic potential of sigma-1 receptor ligands. *Curr Neuropharmcol*. 2008, 6, 344-366.
5. de la Puente, B.; Nadal, X.; Portillo-Salido, E.; Sánchez-Arroyos, R.; Ovalle, S.; Palcios, G.; Muro, A.; Romero, L.; Entrena, J. M.; Baeyens, J. M.; Lôpez-García, J. A.; Maldonado, R.; Zamanillo, D.; Vela, J. M. Sigma-1 receptors regulate activity-induced spinal sensitization and neuropathic pain after peripheral nerve injury. *Pain*. 2009, 145, 294-303.
6. Drews, E.; Zimmer, A. Central sensitization needs sigma receptors. *Pain.* 2009, 145, 269-270.

7. Hanner M., Moebius, F. F., Flandorfer, A.; Knaus, H. G.; Striessnig, J.; Kempner, E.; Glossmann, H. Purification, molecular cloning, and expression of mammalian σ1-binding site. *Proc. Natl. Acad. Sci. USA*. 1996, 93, 8072-8077.
8. James, M. L.; Shen, B.; Nielsen, C. H.; Behera, D.; Buckmaster, C. L.; Mesangeau, C.; Zavaleta, C.; Vuppala, P. K.; Jamalapuram, S.; Avery, B. A.; Lyons, D. M.; McCurdy, C. R.; Biswal, S.; Gambhir, S. S.; Chin, F. T. Evaluation of σ-1 receptor radioligand ^{18}F-FTC-146 in rats and squirrel monkeys using PET. *J Nucl Med*. 2014, 55, 147-153.
9. James, M. L.; Shen, B.; Zavaleta, C. L.; Nielsen, C. H.; Mesangeau, C.; Vuppala, P. K.; Chan, C.; Avery, B. A.; Fishback, J. A.; Matsumoto, R. R.; Gambhir, S. S.; McCurdy, C. R.; Chin, F. T. New positron emission tomography (PET) radioligand for imaging sigma-1 receptors in living subjects. *J Med Chem.* 2012, 55, 8272-8282.
10. Jarvik, J. G.; Yuen, E.; Kliot, M. Diagnosis of carpal tunnel syndrome: electrodiagnostic and MR imaging evaluation. *Neuroimag Clin N Am*. 2004, 14, 93-102.
11. Martin, W. R.; Eades, C. G.; Thompson, J. A.; Huppler, R. E.; Gilbert, P. E. The effects of morphine- and nalorphine-like drugs in the nondependent and morphine-dependent chronic spinal dog. *J. Pharmacol. Exp. Thera*. 1976, 197, 517-532.
12. Maurice, T.; Su, T. P. The pharmacology of sigma-1 receptors. *Pharmacol. Ther.* 2009, 124, 195-206.

13. Mei, J.; Pasternak, G. W. Molecular cloning and pharmacological characterization of the rat σ1 receptor. *Biochem. Pharmacol*. 2001, 62, 349-355.

14. Muehllehner, G.; Karp, J. S. Positron emission tomography. *Phys. Med. Biol*. 2006, 51, 117-137.

15. Narayanan, S.; Bhat, R.; Mesangeau, C.; Poupaert, J. H.; McCurdy, C. R. Early development of sigma-receptor ligands. *Future Med. Chem*. 2011, 3, 79-94.

16. Pan, Y. X.; Mei, J.; Xu, J.; Wan, B. L.; Zuckermann, A.; Pasternak, G. W. Cloning and characterization of a mouse σ1 receptor. *J. Neurochem*. 1998, 70, 2279-2285.

17. Phelps, M. E. Positron emission tomography provides molecular imaging of biological processes. *Proc. Natl. Acad. Sci. U.S.A.*. 2000, 97, 9226-9233.

18. Pike, V. W. PET radiotracers: crossing the blood-brain barrier and surviving metabolism. *Trends Pharmacol Sci*. 2009, 30, 341-440.

19. Seth, P.; Fei, Y. J.; Li, H. W.; Huang, W.; Leibach, F. H.; Ganapathy, V. Cloning and functional characterization of a σ receptor from rat brain. *J. Neurochem*. 1998, 70, 922-931.

20. Seth, P.; Leibach, F. H.; Ganapathy, V. Cloning and structural analysis of the cDNA and the gene encoding the murine type 1 σ receptor. *Biochem. Biophys. Res. Commun.* 1997, 241, 535-540.

21. Shen, B.; Behera, D.; James, M. L.; Borogohain, P.; Andrews, L.; Lutz, A. B.; Mavlyutov, T.; Patankar, M.; Puoho, A. E.; McCurdy, C. R.; Gambhir, S. S.; Biswal, S.; Chin, F. T. Identifying peripheral pain generators via PET/MR imaging. *Proc. Natl. Acad. Sci. U.S.A.*. 2015.

22. Tsai, S. Y.; Hayashi, T.; Mori,T.; Su, T. P. Sigma-1 receptor chaperones and diseases. *Cent Nerv Syst Agents Med Chem*. 2009, 9, 184-189.

23. Wong, E. H. F.; Knight, A. R.; Woodruff, G. N. [3H] MK-801 labels a site on the N-methyl-D-aspartate receptor channel complex in rat brain membranes. *J. Neurochem.* 1988, 50, 274-281.

24. Yous, S.; Wallez, V.; Belloir, M.; Caignard, D. H.; McCurdy, C. R.; Poupaert, J. H. Novel 2(3H)-benzothiazolones as highly potent and selective sigma-1 receptor ligands. *Med. Chem. Res*. 2005, 14, 158-168.

APPENDIX A: NUCLEAR MAGNETIC RESONANCE SPECTRA

M8

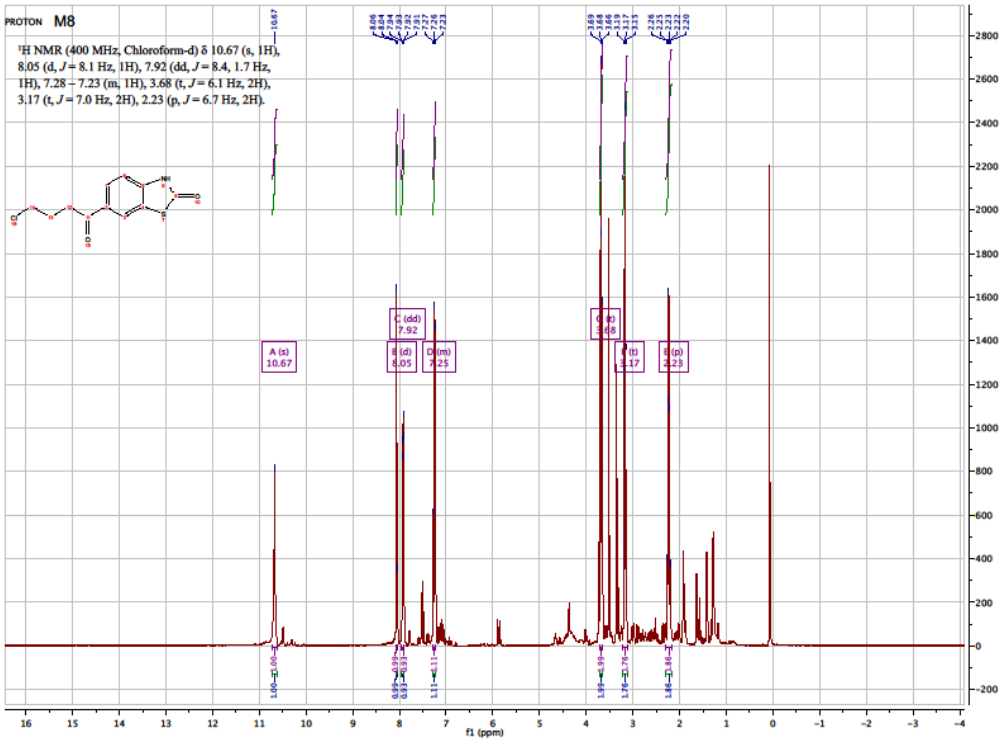

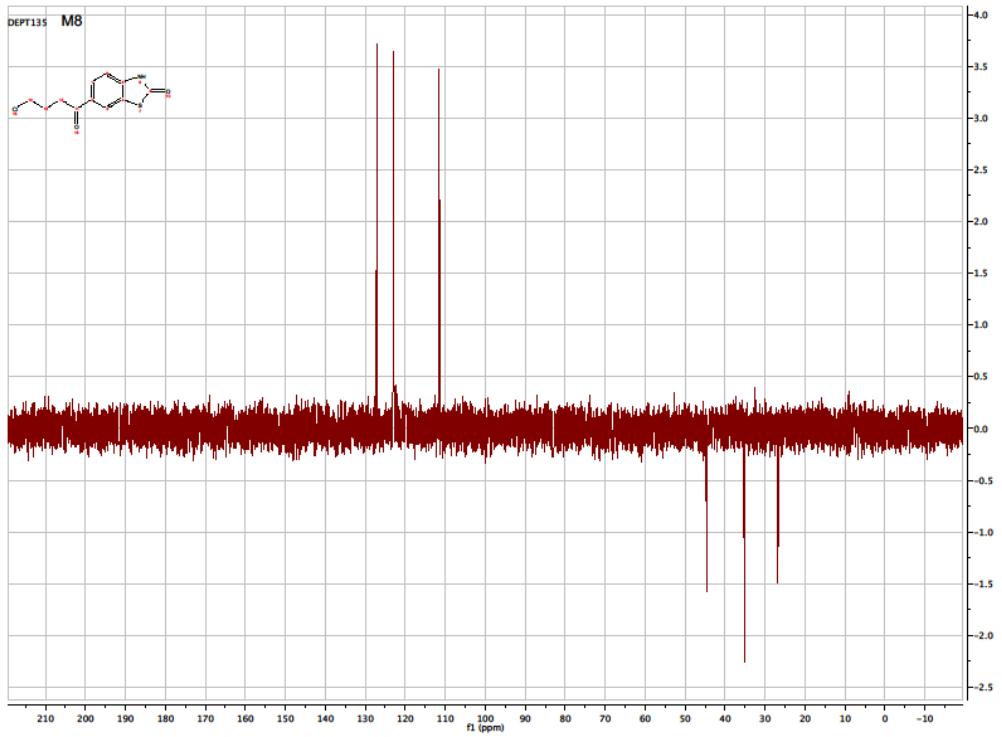

M9

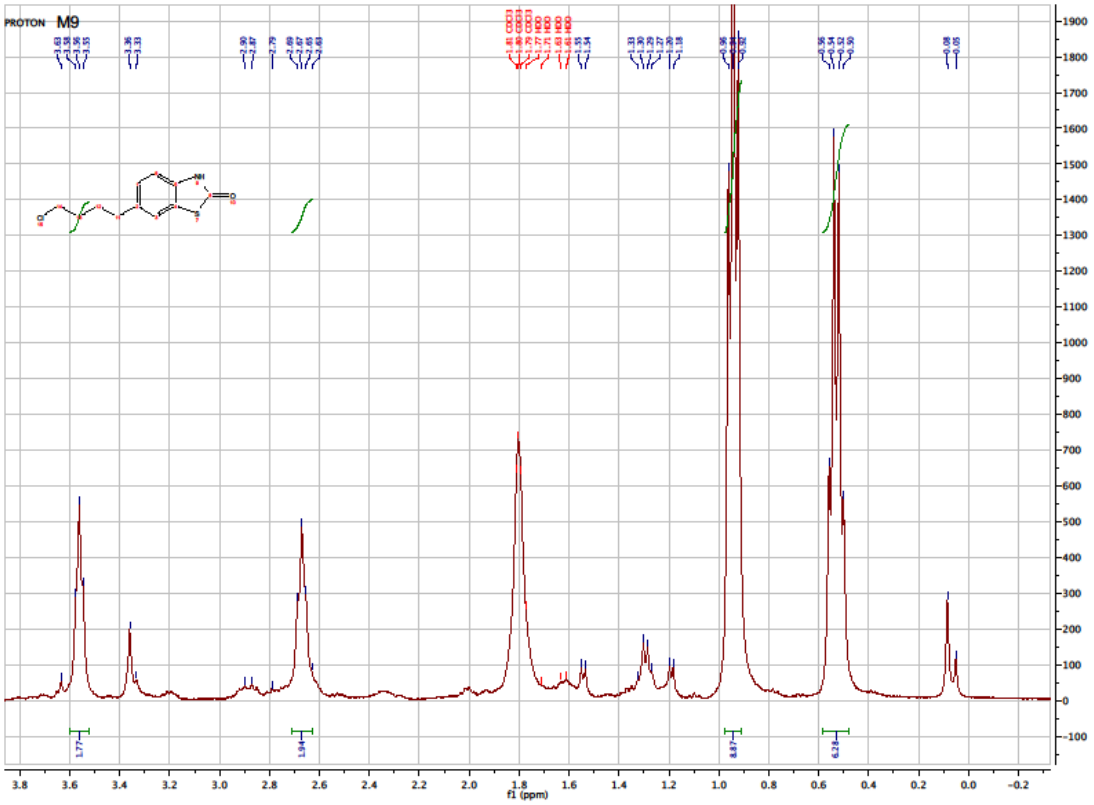
PROTON M9
f1 (ppm)

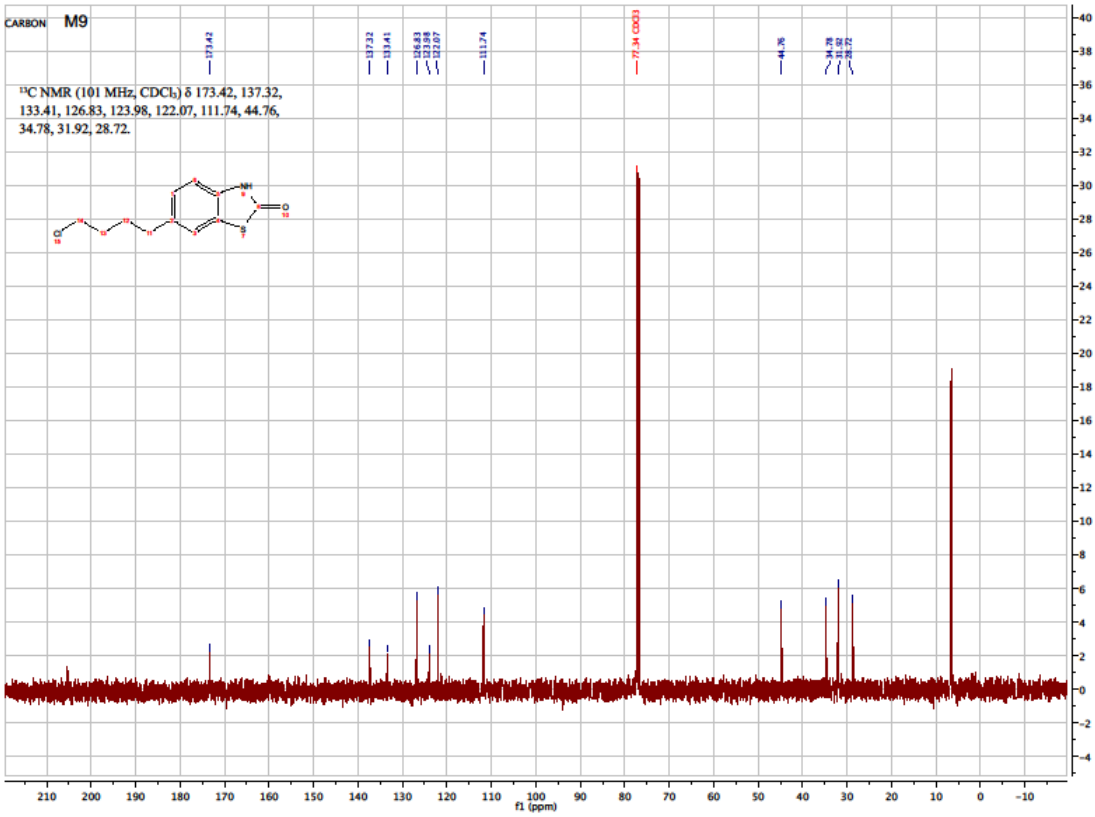
CARBON M9
^{13}C NMR (101 MHz, $CDCl_3$) δ 173.42, 137.32, 133.41, 126.83, 123.98, 122.07, 111.74, 44.76, 34.78, 31.92, 28.72.
f1 (ppm)

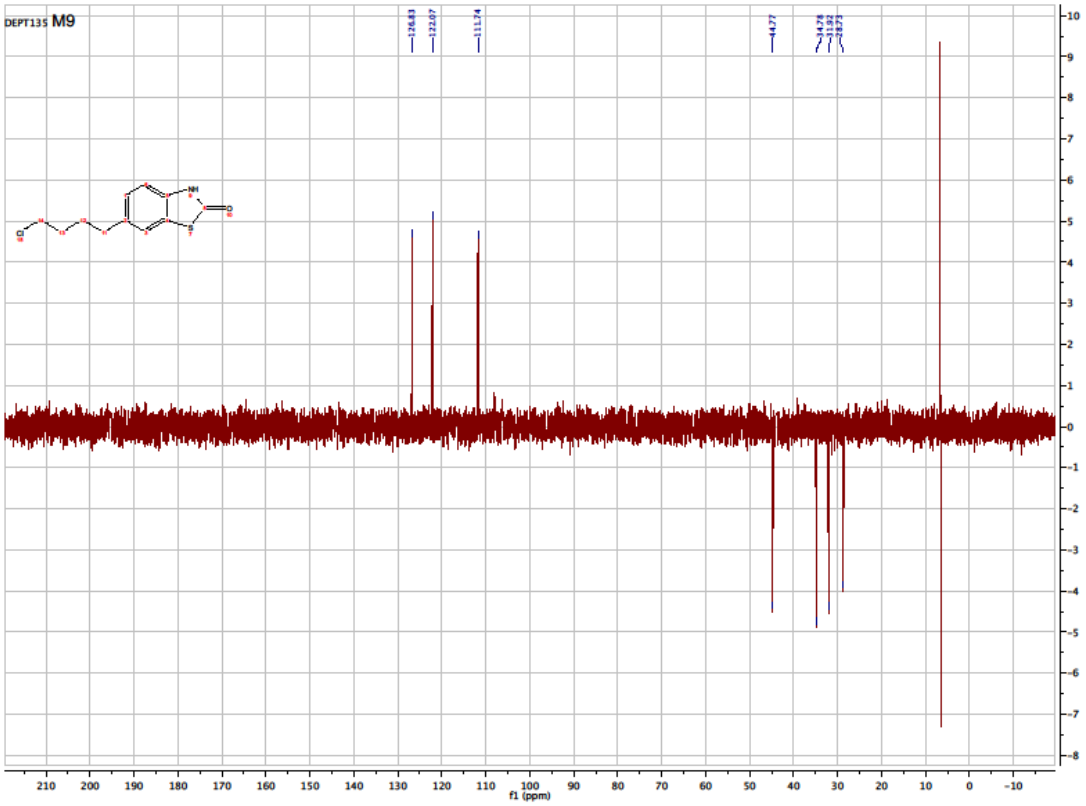
DEPT135 M9
126.83
122.07
111.74
44.77
31.78
31.22
28.73
f1 (ppm)

M10

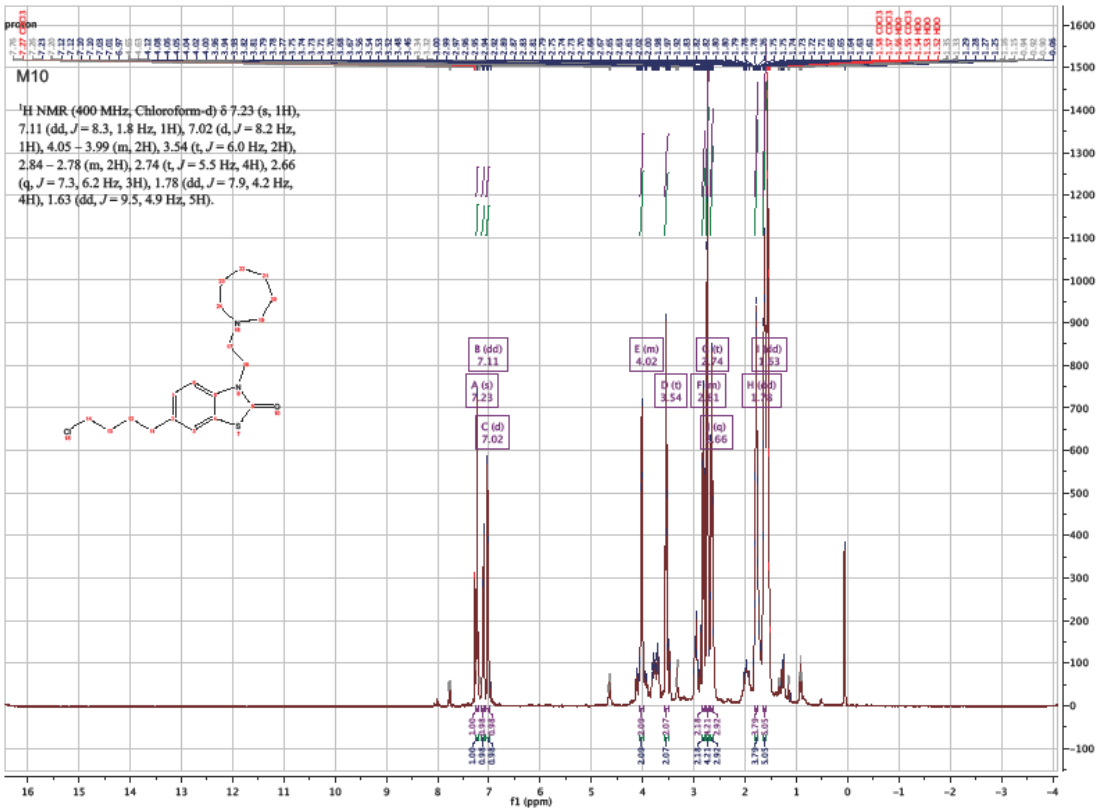
M10
¹H NMR (400 MHz, Chloroform-d) δ 7.23 (s, 1H), 7.11 (dd, J = 8.3, 1.8 Hz, 1H), 7.02 (d, J = 8.2 Hz, 1H), 4.05 – 3.99 (m, 2H), 3.54 (t, J = 6.0 Hz, 2H), 2.84 – 2.78 (m, 2H), 2.74 (t, J = 5.5 Hz, 4H), 2.66 (q, J = 7.3, 6.2 Hz, 3H), 1.78 (dd, J = 7.9, 4.2 Hz, 4H), 1.63 (dd, J = 9.5, 4.9 Hz, 5H).
f1 (ppm)

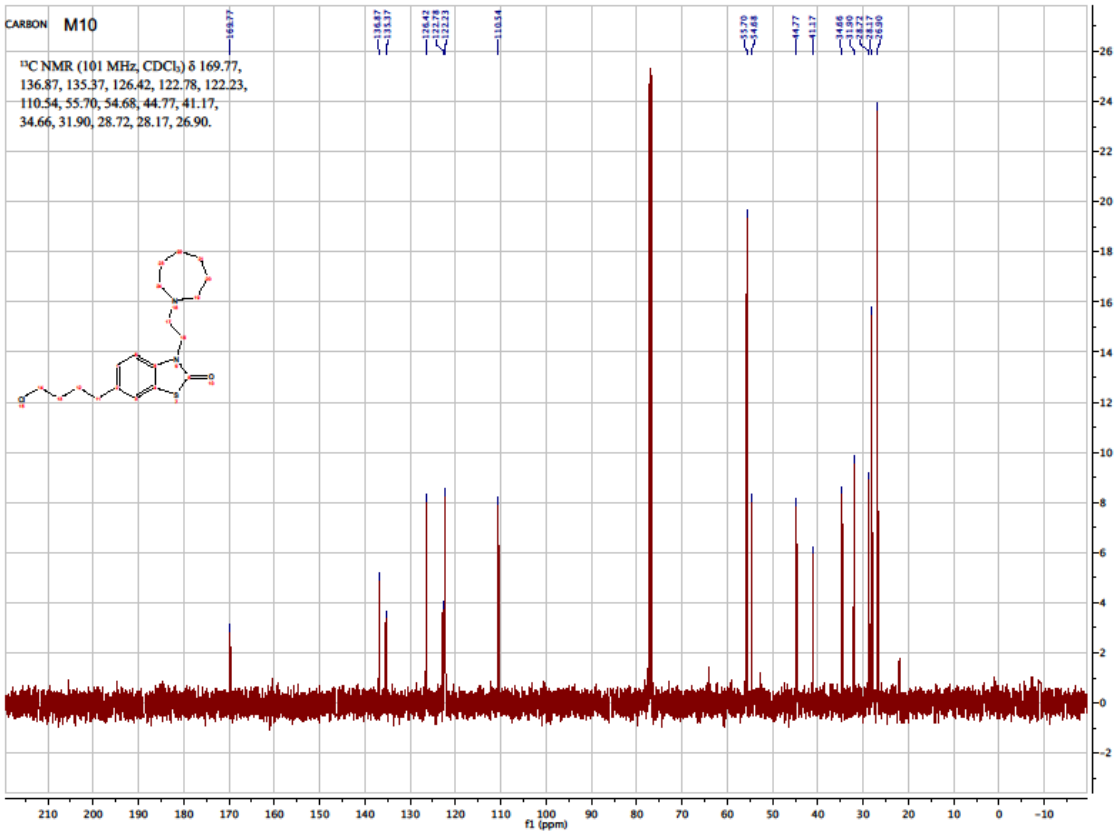
CARBON
M10
^{13}C NMR (101 MHz, $CDCl_3$) δ 169.77, 136.87, 135.37, 126.42, 122.78, 122.23, 110.54, 55.70, 54.68, 44.77, 41.17, 34.66, 31.90, 28.72, 28.17, 26.90.
f1 (ppm)

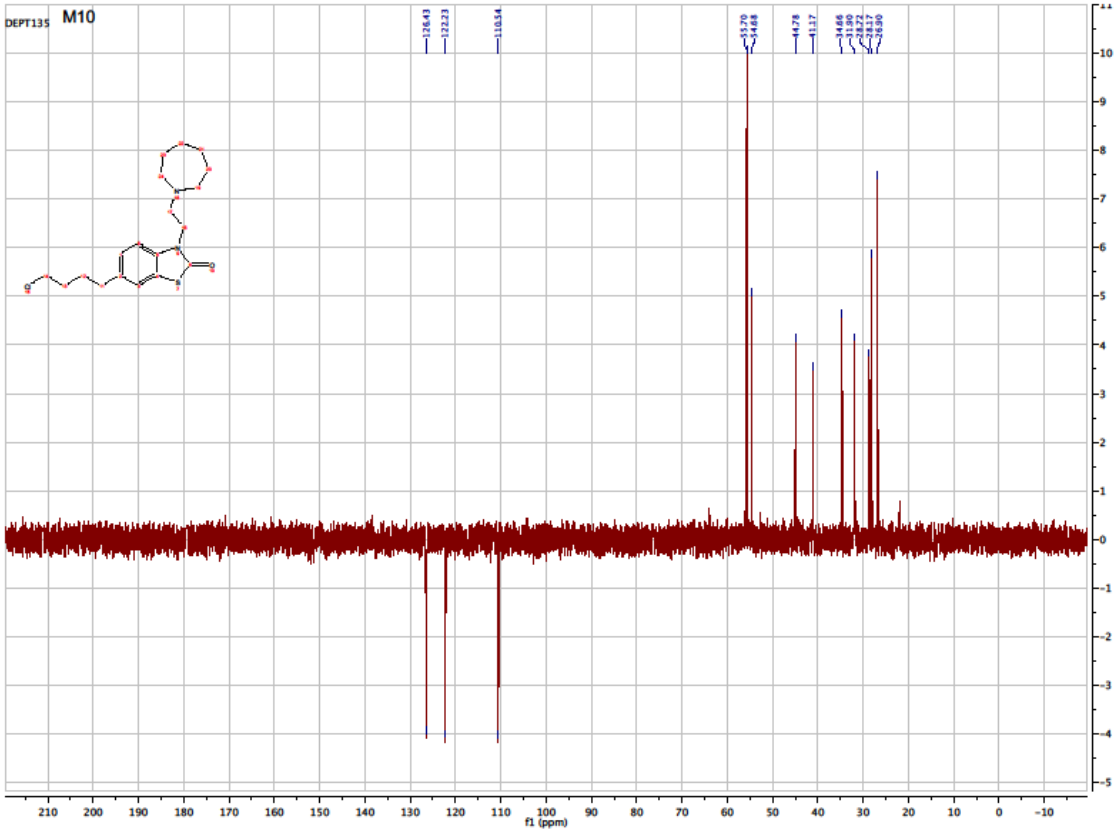
DEPT135
M10
f1 (ppm)

M11

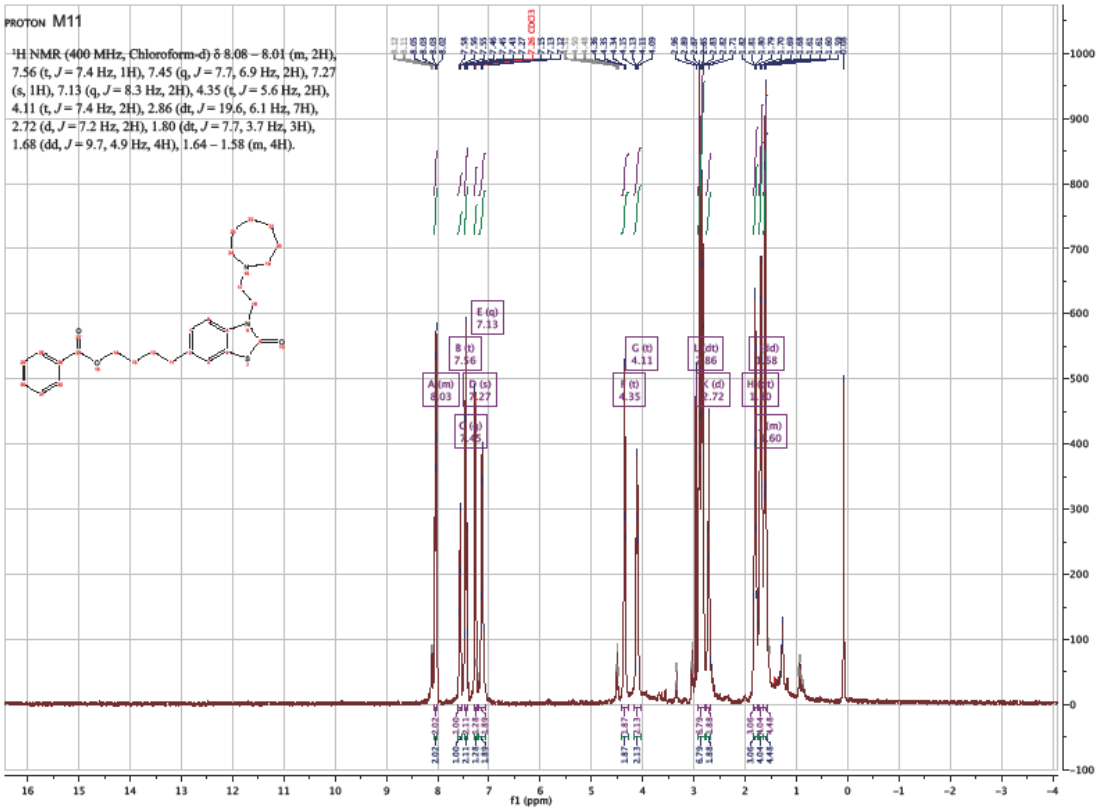
PROTON M11
¹H NMR (400 MHz, Chloroform-d) δ 8.08 – 8.01 (m, 2H), 7.56 (t, J = 7.4 Hz, 1H), 7.45 (q, J = 7.7, 6.9 Hz, 2H), 7.27 (s, 1H), 7.13 (q, J = 8.3 Hz, 2H), 4.35 (t, J = 5.6 Hz, 2H), 4.11 (t, J = 7.4 Hz, 2H), 2.86 (dt, J = 19.6, 6.1 Hz, 7H), 2.72 (d, J = 7.2 Hz, 2H), 1.80 (dt, J = 7.7, 3.7 Hz, 3H), 1.68 (dd, J = 9.7, 4.9 Hz, 4H), 1.64 – 1.58 (m, 4H).
f1 (ppm)

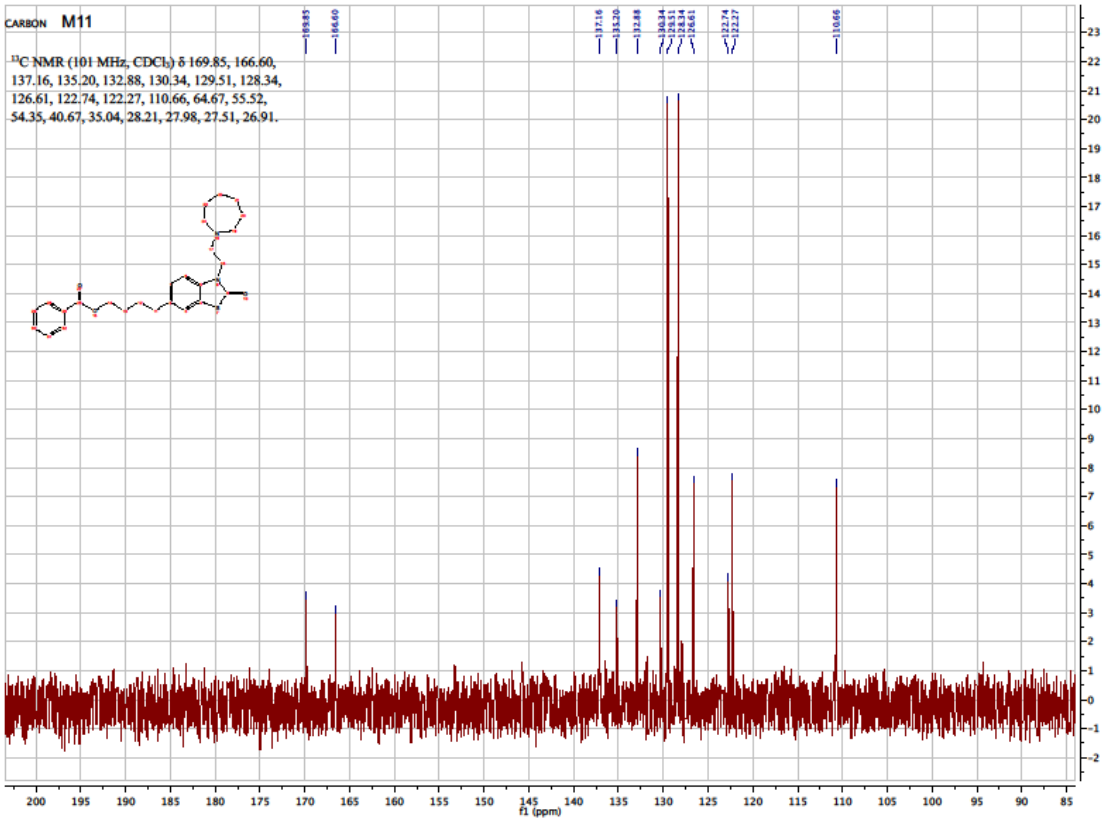
CARBON M11
¹³C NMR (101 MHz, CDCl₃) δ 169.85, 166.60, 137.16, 135.20, 132.88, 130.34, 129.51, 128.34, 126.61, 122.74, 122.27, 110.66, 64.67, 55.52, 54.35, 40.67, 35.04, 28.21, 27.98, 27.51, 26.91.
f1 (ppm)

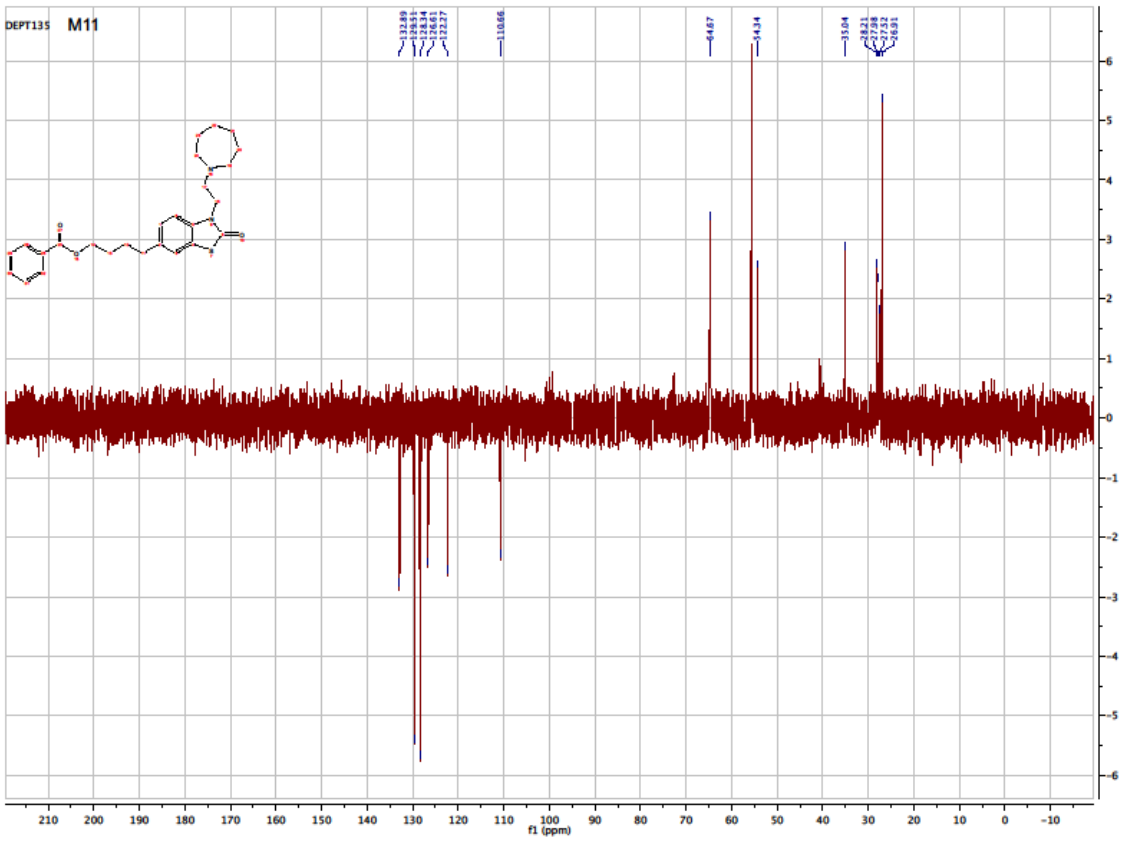
DEPT135 M11
f1 (ppm)

M12

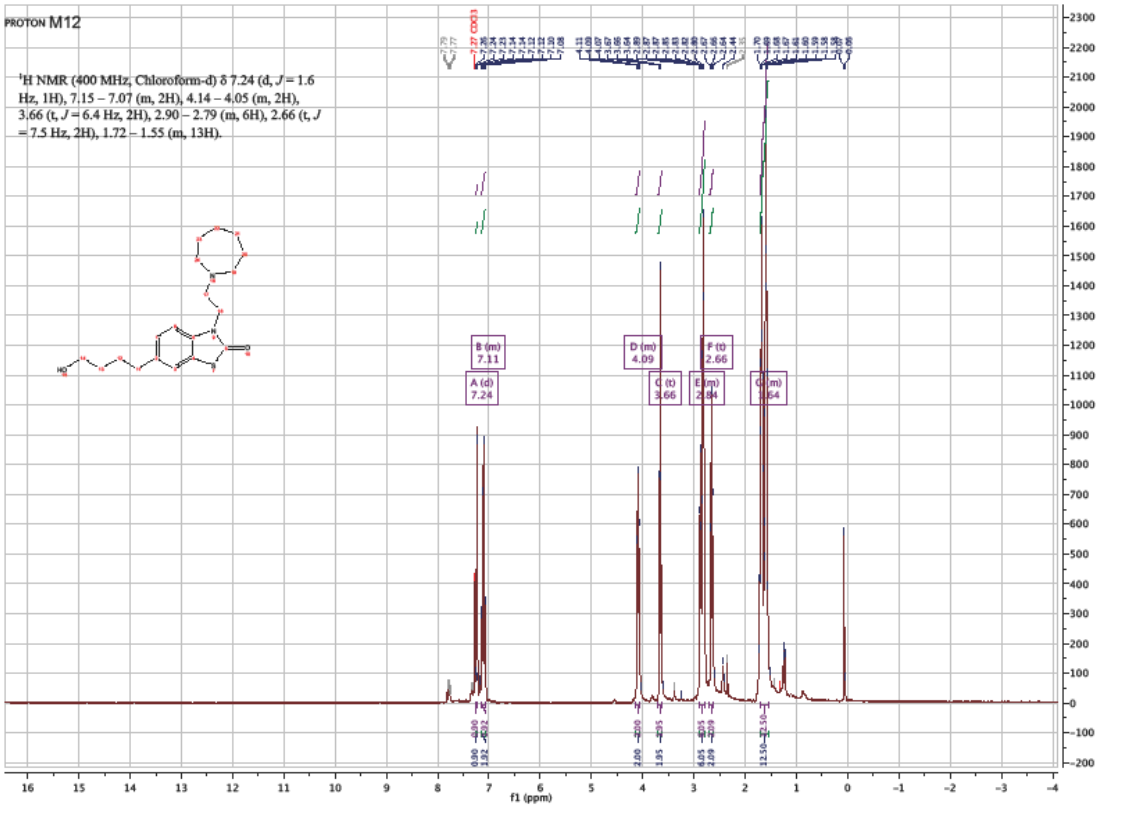
PROTON M12
¹H NMR (400 MHz, Chloroform-d) δ 7.24 (d, J = 1.6 Hz, 1H), 7.15 – 7.07 (m, 2H), 4.14 – 4.05 (m, 2H), 3.66 (t, J = 6.4 Hz, 2H), 2.90 – 2.79 (m, 6H), 2.66 (t, J = 7.5 Hz, 2H), 1.72 – 1.55 (m, 13H).
f1 (ppm)

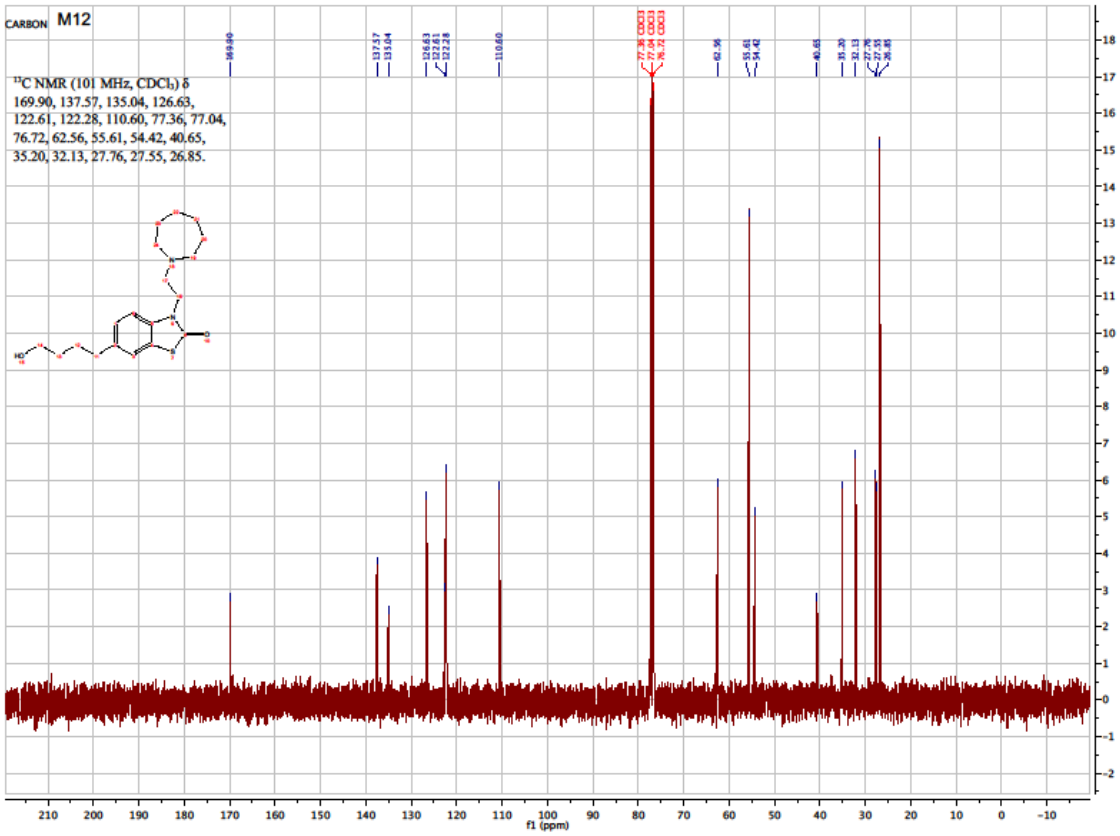
CARBON M12
169.90
137.57
135.04
126.63
122.61
122.28
110.60
77.36 CDCl3
77.04 CDCl3
76.72 CDCl3
62.56
55.61
54.42
40.65
35.20
32.13
27.76
27.55
26.85
13C NMR (101 MHz, CDCl3) δ
169.90, 137.57, 135.04, 126.63,
122.61, 122.28, 110.60, 77.36, 77.04,
76.72, 62.56, 55.61, 54.42, 40.65,
35.20, 32.13, 27.76, 27.55, 26.85.
f1 (ppm)

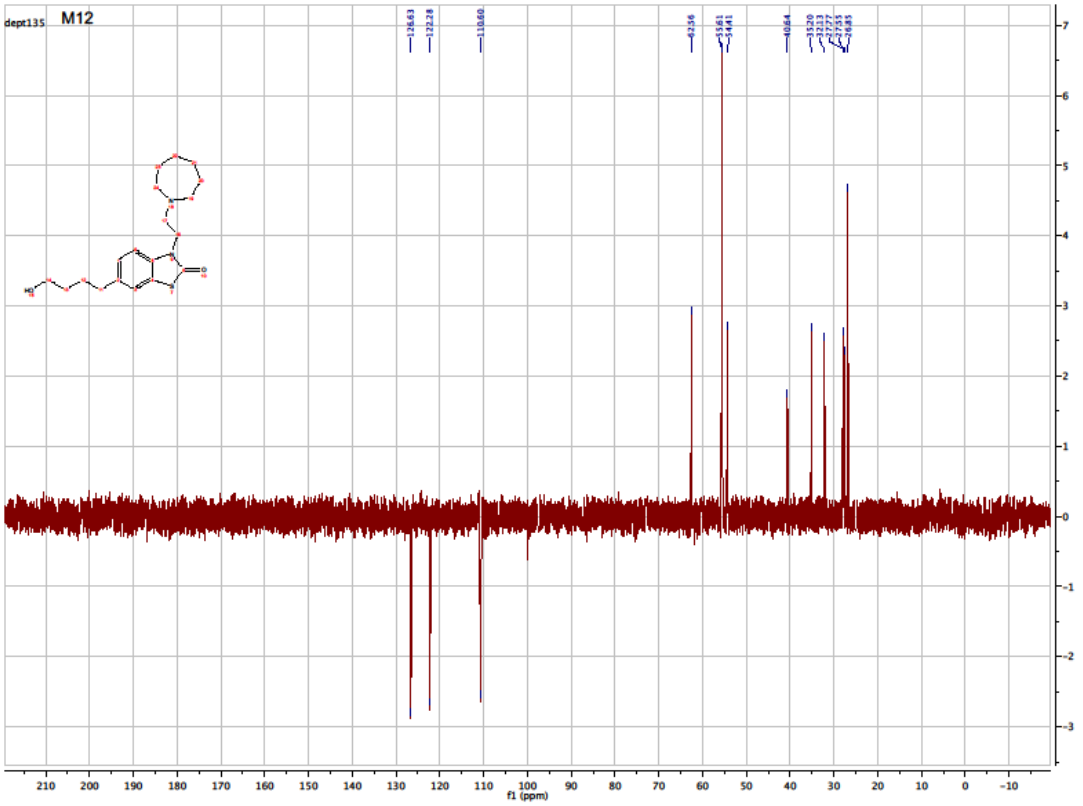
dept135 M12
126.63
122.28
110.60
62.56
55.61
54.41
40.64
35.20
32.13
27.76
27.55
26.85
f1 (ppm)

M13

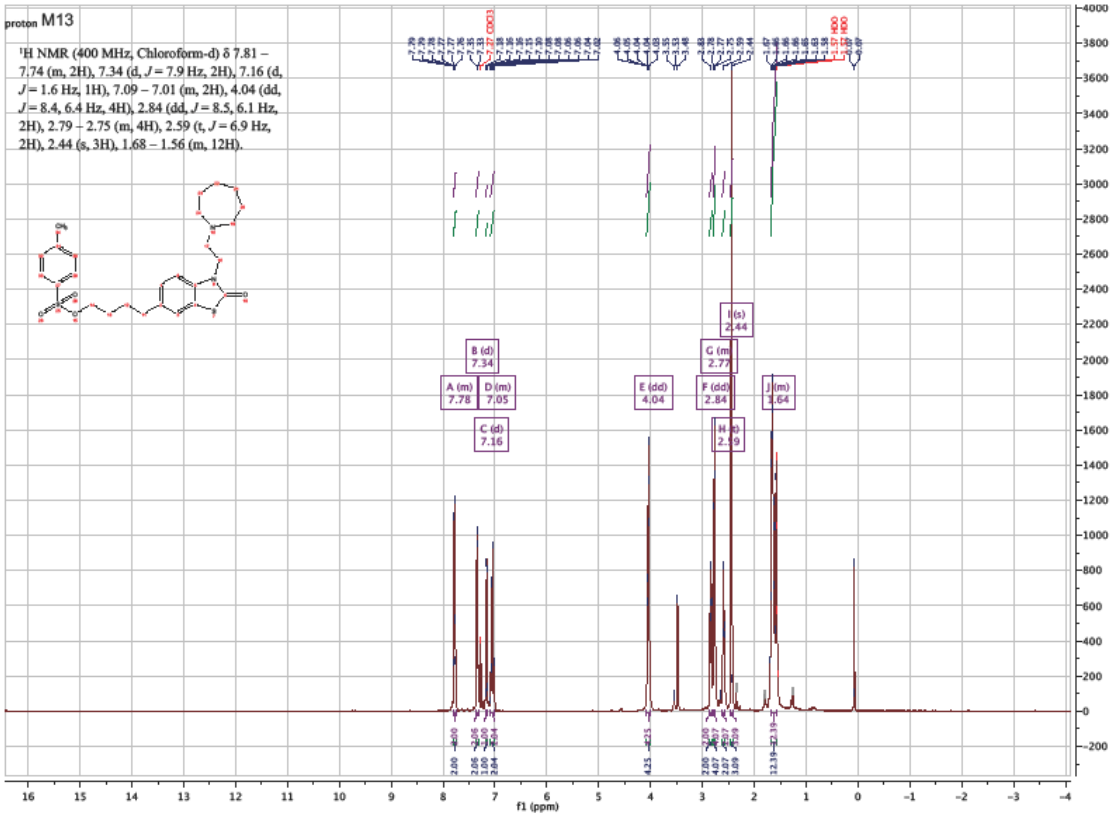
proton M13
¹H NMR (400 MHz, Chloroform-d) δ 7.81 – 7.74 (m, 2H), 7.34 (d, J = 7.9 Hz, 2H), 7.16 (d, J = 1.6 Hz, 1H), 7.09 – 7.01 (m, 2H), 4.04 (dd, J = 8.4, 6.4 Hz, 4H), 2.84 (dd, J = 8.5, 6.1 Hz, 2H), 2.79 – 2.75 (m, 4H), 2.59 (t, J = 6.9 Hz, 2H), 2.44 (s, 3H), 1.68 – 1.56 (m, 12H).
f1 (ppm)

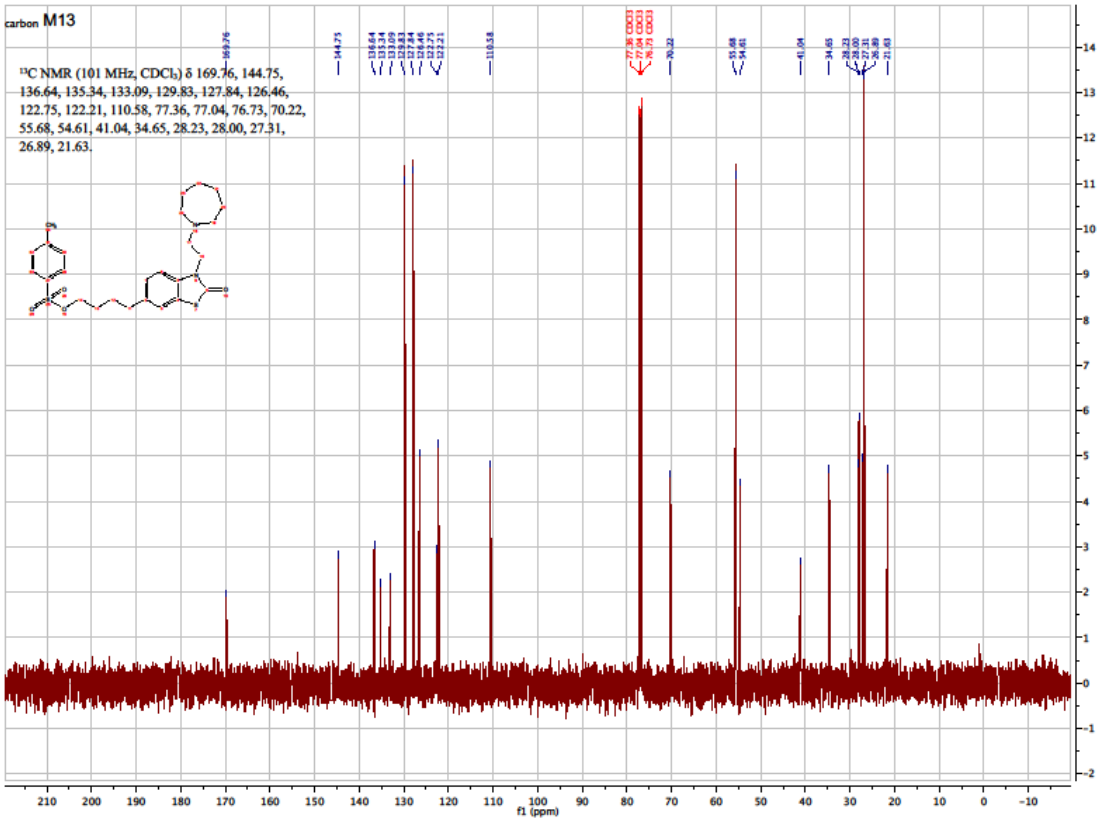
carbon M13
¹³C NMR (101 MHz, CDCl₃) δ 169.76, 144.75, 136.64, 135.34, 133.09, 129.83, 127.84, 126.46, 122.75, 122.21, 110.58, 77.36, 77.04, 76.73, 70.22, 55.68, 54.61, 41.04, 34.65, 28.23, 28.00, 27.31, 26.89, 21.63.
f1 (ppm)

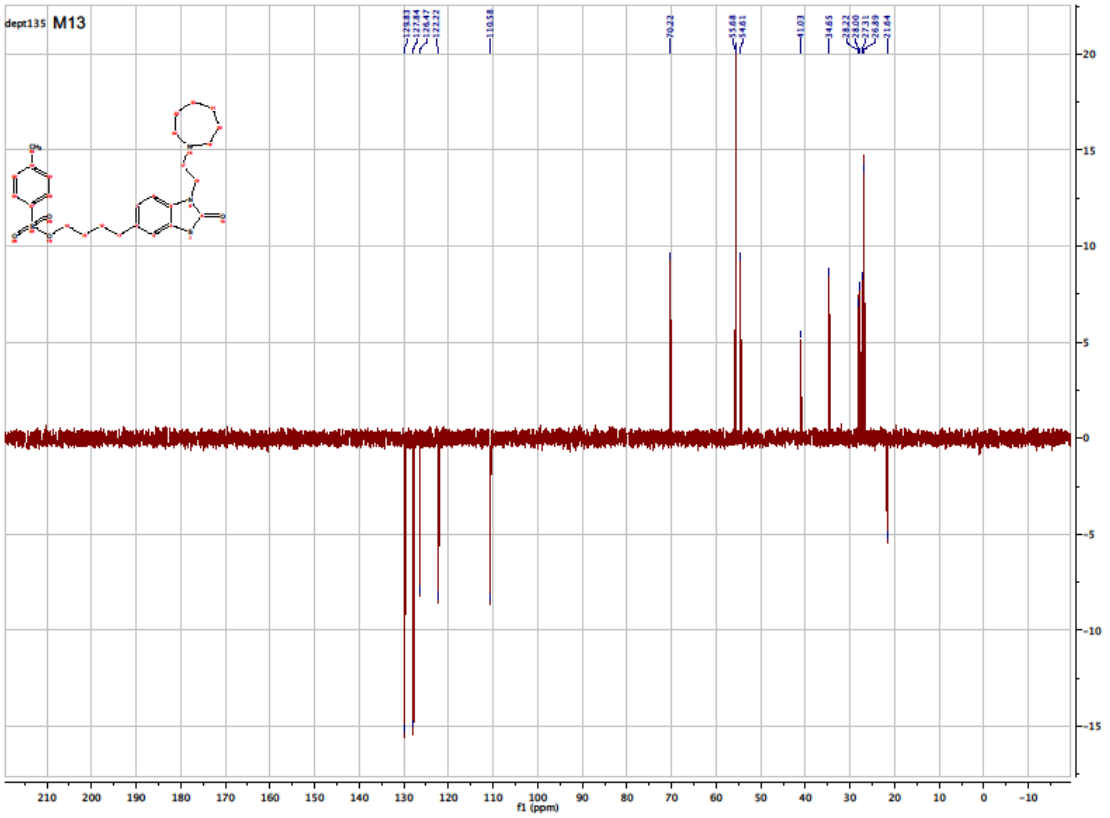
dept135 M13
f1 (ppm)

M14

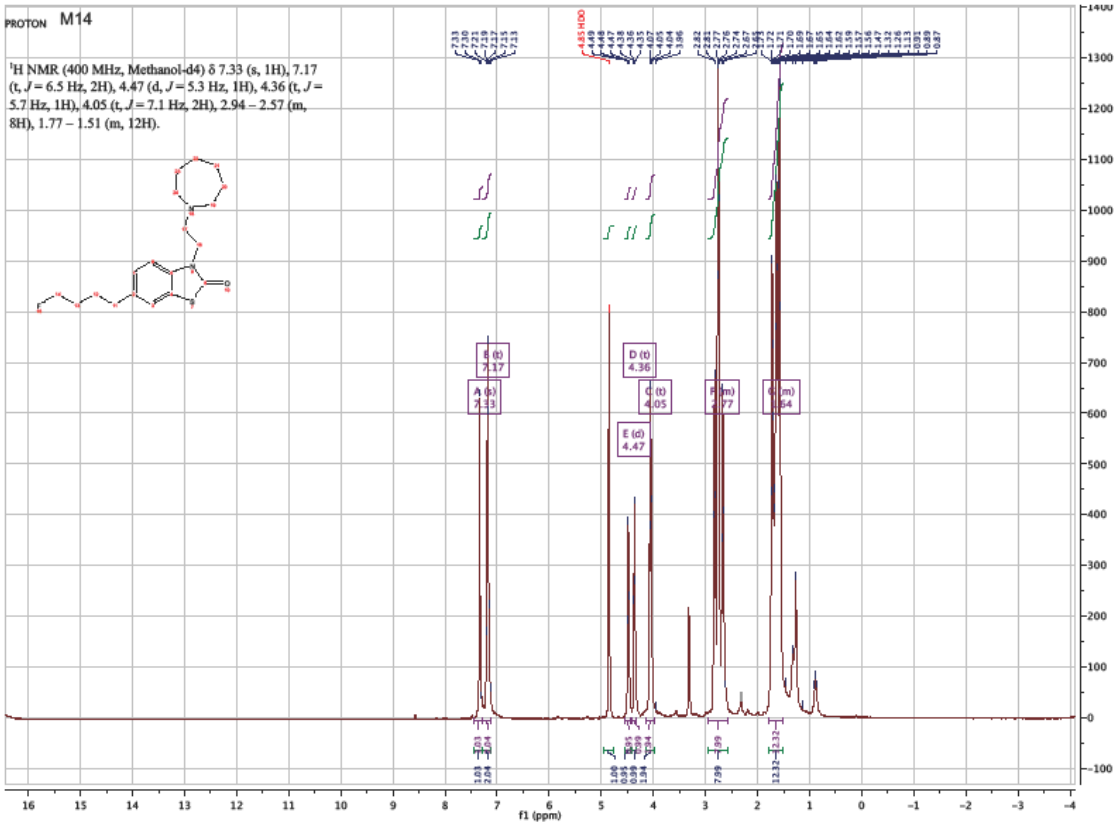
PROTON M14
¹H NMR (400 MHz, Methanol-d4) δ 7.33 (s, 1H), 7.17 (t, J = 6.5 Hz, 2H), 4.47 (d, J = 5.3 Hz, 1H), 4.36 (t, J = 5.7 Hz, 1H), 4.05 (t, J = 7.1 Hz, 2H), 2.94 – 2.57 (m, 8H), 1.77 – 1.51 (m, 12H).
f1 (ppm)

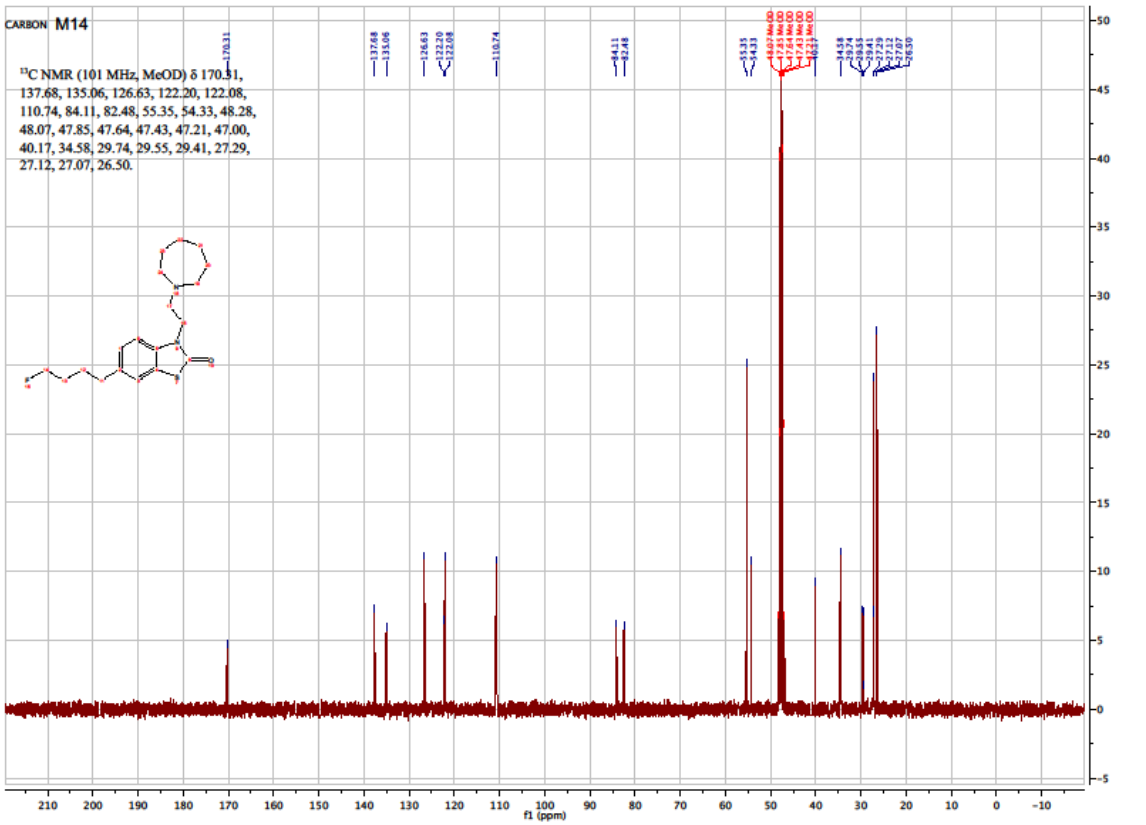
CARBON M14
^{13}C NMR (101 MHz, MeOD) δ 170.31, 137.68, 135.06, 126.63, 122.20, 122.08, 110.74, 84.11, 82.48, 55.35, 54.33, 48.28, 48.07, 47.85, 47.64, 47.43, 47.21, 47.00, 40.17, 34.58, 29.74, 29.55, 29.41, 27.29, 27.12, 27.07, 26.50.
f1 (ppm)

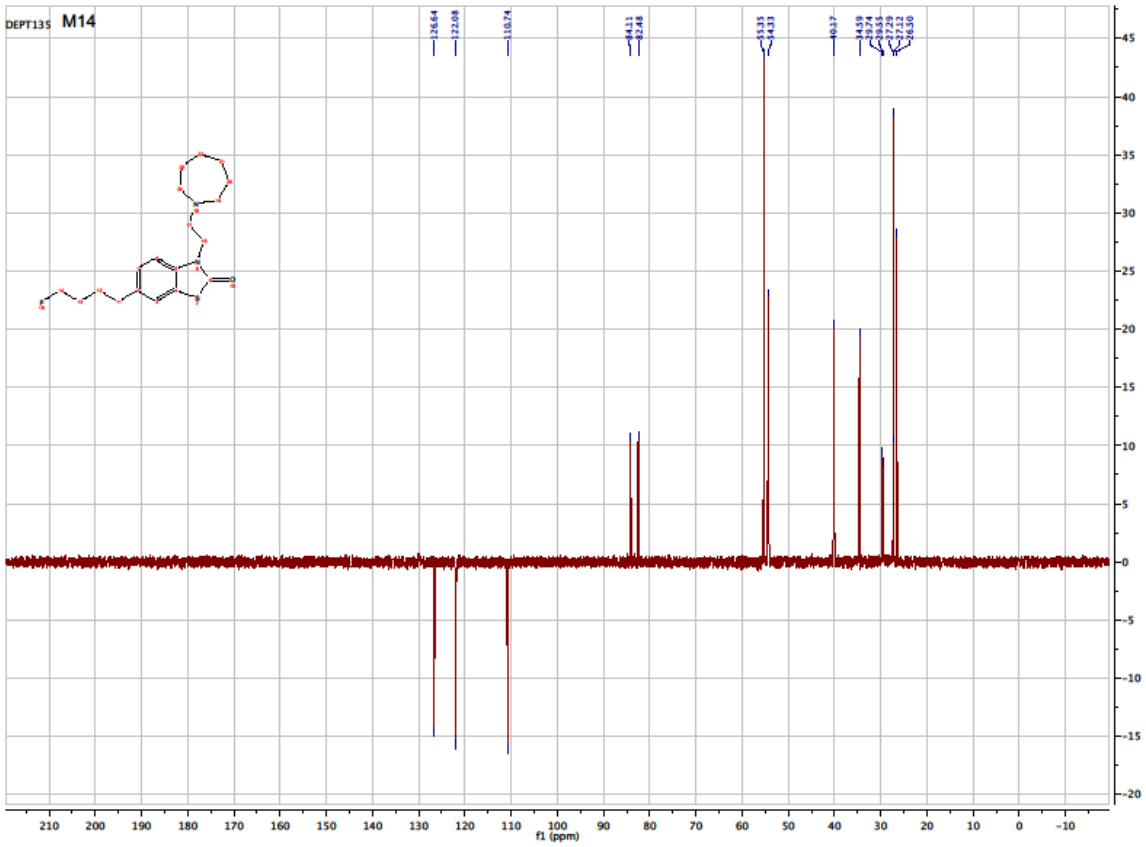
DEPT135 M14
f1 (ppm)

APPENDIX B: MASS SPECTRUM DATA

M8

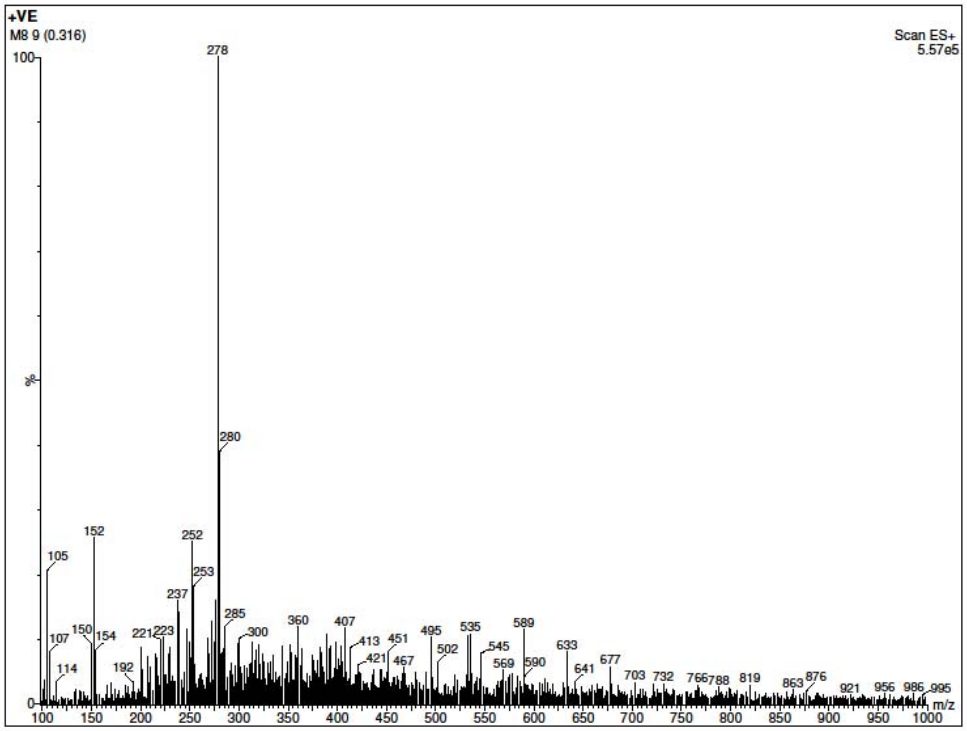

Mass Spectrum for M9 is not available.

M10

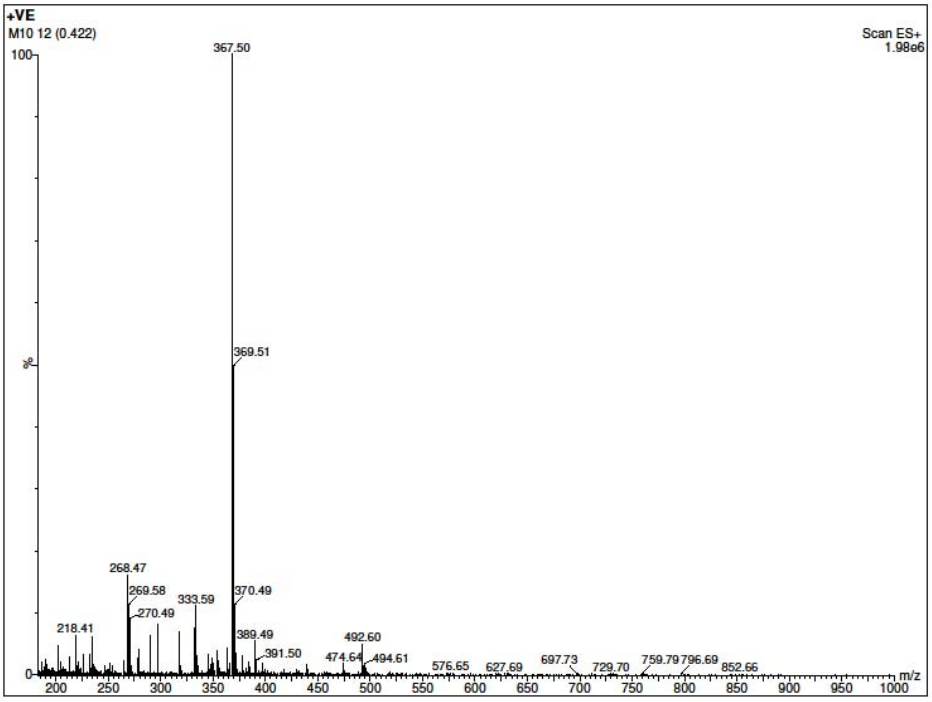
+VE
M10 12 (0.422)
Scan ES+
1.98e6
100
%
0
367.50
369.51
268.47
269.58
270.49
333.59
370.49
218.41
389.49
391.50
492.60
474.64
494.61
576.65
627.69
697.73
729.70
759.79
796.69
852.66
200 250 300 350 400 450 500 550 600 650 700 750 800 850 900 950 1000
m/z

M11

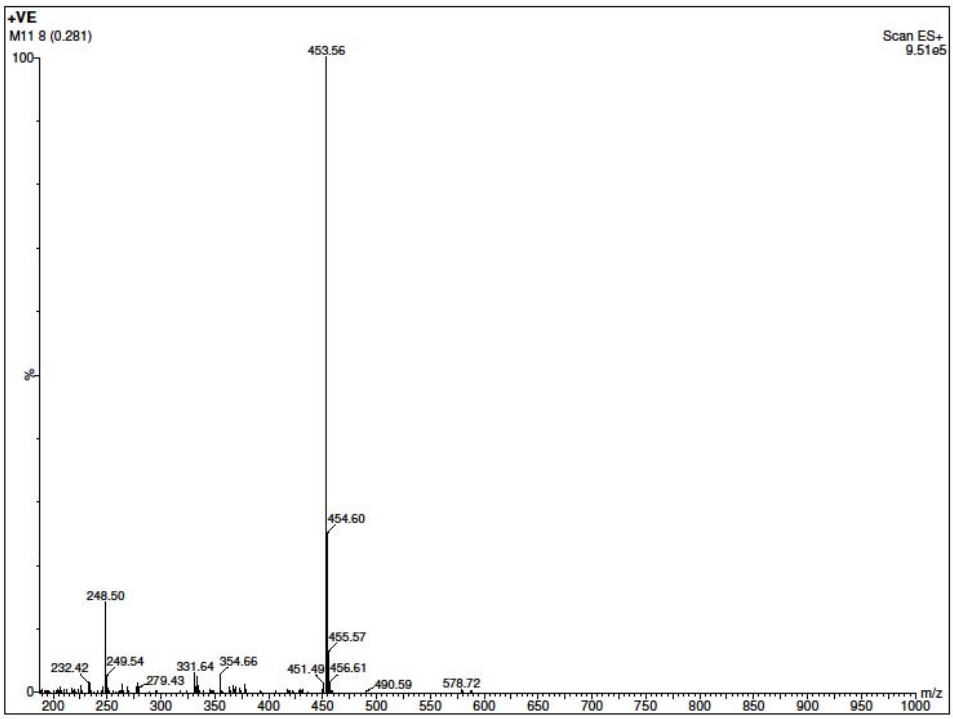
+VE
M11 8 (0.281)
Scan ES+
9.51e5
100
%
0
453.56
454.60
248.50
455.57
232.42
249.54
279.43
331.64
354.66
451.49
456.61
490.59
578.72
200 250 300 350 400 450 500 550 600 650 700 750 800 850 900 950 1000
m/z

M12

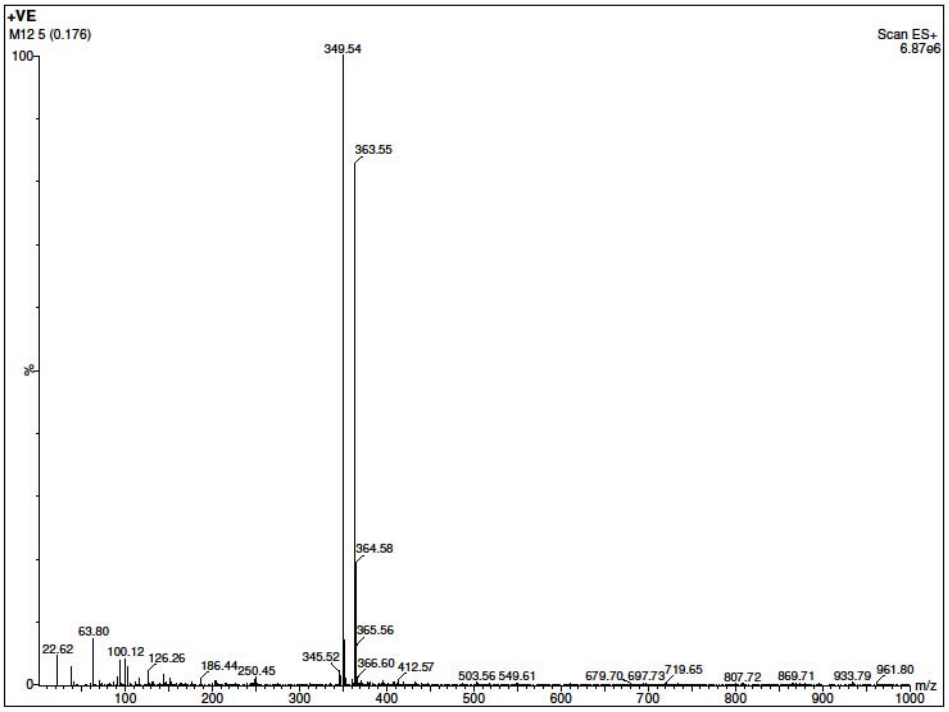
+VE
M12 5 (0.176)
Scan ES+
6.87e6
100
%
0
349.54
363.55
364.58
365.56
366.60
345.52
63.80
22.62
100.12
126.26
186.44
250.45
412.57
503.56
549.61
679.70
697.73
719.65
807.72
869.71
933.79
961.80
100
200
300
400
500
600
700
800
900
1000
m/z

M13

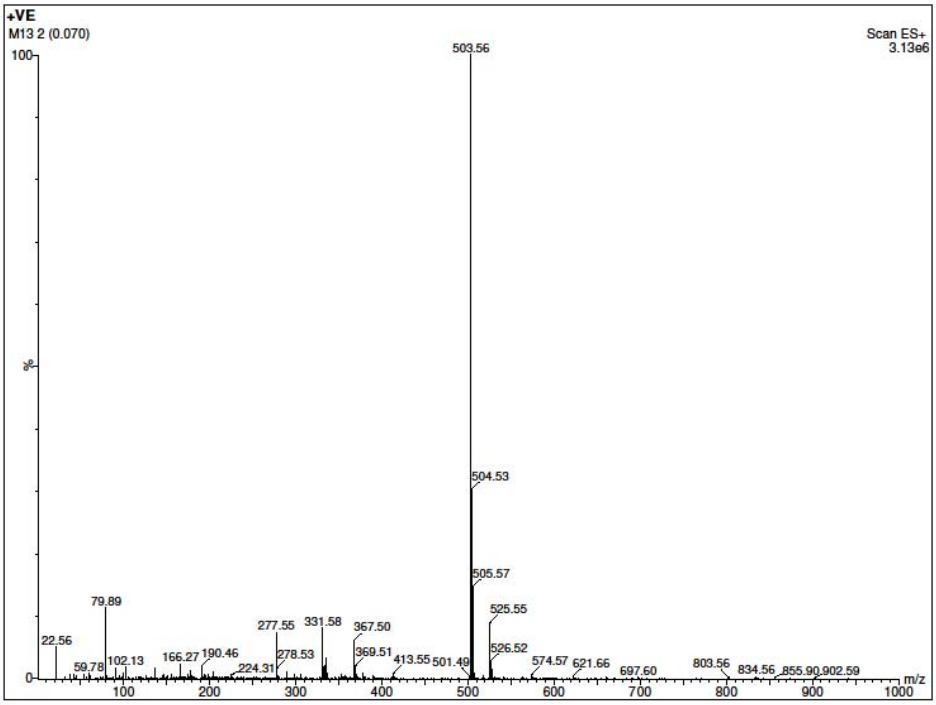
+VE
M13 2 (0.070)
Scan ES+
3.13e6
100
%
0
503.56
504.53
505.57
525.55
526.52
79.89
22.56
59.78
102.13
166.27
190.46
224.31
277.55
278.53
331.58
367.50
369.51
413.55
501.49
574.57
621.66
697.60
803.56
834.56
855.90
902.59
100
200
300
400
500
600
700
800
900
1000
m/z

M14

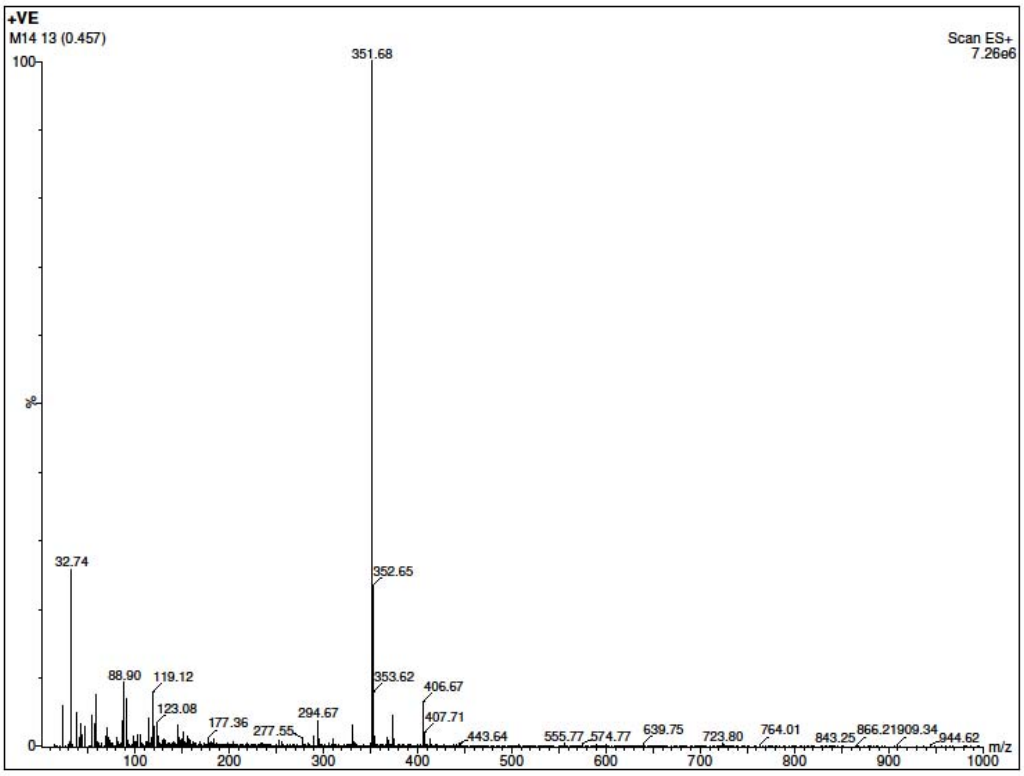
+VE
M14 13 (0.457)
Scan ES+
7.26e6
100
%
0
351.68
352.65
32.74
88.90
119.12
123.08
177.36
277.55
294.67
353.62
406.67
407.71
443.64
555.77
574.77
639.75
723.80
764.01
843.25
866.21
909.34
944.62
100
200
300
400
500
600
700
800
900
1000
m/z